INTEGRATED METHOD TO EVALUATE ACID STIMULATION OF HORIZONTAL WELLS IN CARBONATE RESERVOIR THROUGH TREATMENT PRESSURE ANALYSIS

A Thesis

by

KENJI UEDA

Submitted to the Office of Graduate and Professional Studies of
Texas A&M University
in partial fulfillment of the requirements for the degree of

MASTER OF SCIENCE

Chair of Committee,	Ding Zhu
Committee Members,	A. Daniel Hill
	Marcelo Sanchez
Head of Department,	A. Daniel Hill

August 2015

Major Subject: Petroleum Engineering

ABSTRACT

Unlocking a tight carbonate formation for oil and gas production by multi-stage acid stimulation is a relatively cost-effective method as an alternative to propped fracturing for production enhancement. Depending on whether treatment pressure is below or above the formation closure stress, acid stimulation is basically divided into matrix acidizing and acid fracturing. In this study, practical methodology to evaluate both matrix acidizing and acid fracturing through treatment monitoring is presented respectively.

For matrix acidizing, monitoring and optimizing a matrix acidizing has been achieved by integrating a forward model used in acidizing design for horizontal wells with a real-time monitoring model for skin evolution during the stimulation. The effect of acidizing is described as an overall skin factor change, and productivity improvement is predicted for the treatment. Then the field treatment data monitored on-site was used to estimate the skin response by treatment injection. History matching procedure of design and actual treatment data will be carried out to update near-wellbore and key wormholing parameters. Through sensitivity study, which parameter should be updated is discussed. Finally optimum rate schedule is identified based on updated parameters.

Meanwhile, for acid fracturing treatment, new method for real-time monitoring of acid fracturing, the inverse injectivity vs. superposition time function plot is proposed, subject to the condition that the treatment pressure is above closure pressure after the breakdown. Combining a linear dual-porosity transient slab model with injectivity concept, actual growing cross-sectional area induced by acid fracturing treatment can be monitored

in real-time. After production starts, linear flow diagnostic approach with rate-transient analysis provides cross-sectional area flowing from matrix, which is compared with the area induced by acid fracturing during the stimulation. The treatment efficiency provides engineers with additional information as to whether the designed acid fracturing was performed appropriately under the in-situ closure stress field.

A field case example of both multi-stage matrix acidizing and acid fracturing acid in horizontal well are also presented respectively in the study to illustrate the application of the approach developed, and to show the value of the integrated approach to monitor and diagnose acid stimulation in horizontal wells.

DEDICATION

To my wife, Risako, little one, Riku and unborn baby.

ACKNOWLEDGEMENTS

I would like to thank my committee chair, Dr. Zhu, and my committee members, Dr. Hill, and Dr. Sanchez, for their guidance and support throughout the course of this research.

Thanks also go to my colleagues in room 714 for making my time at Texas A&M University a great experience. I also want to extend my gratitude to Nozomu Yoshida for his help with friendship and brain-storming through a coffee break.

Finally, I thank my wife, Risako, for her patience, encouragement and love, and my little one, Riku, for making our life fun in College Station. I could not have completed without their support.

NOMENCLATURE

A	pipe cross-sectional area, L^2, ft^2
A_c	cross-sectional area to flow, ft^2
A_{cm}	total matrix surface area draining into fracture system, ft^2
B	formation volume factor, L^3/L^3, RB/STB
b	intercept of linear function between flow rate, pressure and time
c_t	total compressibility, $M^{-1}L\text{-}1T^2$, psi^{-1}
D	tubing inner diameter, L, inch
$d_{e,wh}$	effective wormhole radius, L, ft
d_{perf}	perforation diameter, L, in.
$f(u)$	relation used in Laplace space to distinguish matrix geometry
f_f	fanning friction factor, dimensionless
g	acceleration of gravitation, LT^{-2}, ft/sec^2
g_c	gravitational dimensional constant
h	thickness, L, ft
h	reservoir thickness, ft.
h_{perf}	perforation spacing, L, ft.
h_s	coordinate of wellbore location in z-direction
h_{wh}	wormhole axial spacing, L, ft.
h_x	length of the flow field modeled
h_z	height of the flow field modeled

I_{ani}	anisotropy ratio, dimensionless
k	permeability, L^2, md
K'	Fluid-consistency index
K_d	Perforation coefficient
k_f	bulk fracture permeability of dual porosity models, md
k_H	horizontal permeability, L^2, md
k_m	matrix permeability, md
k_s	damage permeability, L^2, md
k_V	vertical permeability, L^2, md
k_x	permeability in x-direction
k_y	permeability in y-direction
k_z	permeability in z-direction
L	length, L, ft
l	half of fracture spacing, ft.
L	general fracture spacing, ft.
l^{-1}	inverse Laplace space operator
L_{core}	core length, L, inch
L_w	length of horizontal well
L_{xd}	left coordinate of wellbore in x-direction
L_{xl}	right coordinate of wellbore in x-direction
m	slope of linear function between flow rate, pressure and time
$\tilde{m}^4$	slope of regions 4 (matrix linear flow region)

$m(p)$	pseudopressure (gas), psi^{-2}/cp
m_D	dimensionless psuedo pressure
m_{DL}	dimensionless pressure (rectangular geometry, gas)
m_{wh}	number of dominant wormholes per plane
n'	flow-behavior index
N_{Ac}	acid capacity number, dimensionless
N_{perf}	number of perforations
N_{Re}	reynolds number, dimensionless
p	pressure drop, $ML^{-1}T^{-2}$, psi
p_D	dimensionless pressure, dimensionless
p_{DL}	dimensionless pressure based on rectangular geometry, linear
p_i	initial reservoir pressure, $ML^{-1}T^{-2}$, psi
$PV_{bt,opt}$	optimum pore volume to breakthrough, dimensionless
p_{WDL}	dimensionless pressure based on rectangular geometry, linear
p_{wf}	bottom flowing pressure, $ML^{-1}T^{-2}$, psi
q	flow rate, L^3T^{-1}, ft^3/min
q_g	gas rate, Mscf/day
q_w	flow rate in the wellbore, L3t-1, bbl/min
r_d	damage radius, L, ft
r_w	wellbore radius, L, ft
r_w’	equivalent wellbore radius, L, ft
r_{wh}	wormhole penetration radius, L, ft

s	skin factor, dimensionless
$s_{overall}$	overall skin factor, dimensionless
t	time, hours
T	absolute temperature, oR
t_D	dimensionless time
t_{DAc}	dimensionless time based on Ac (rectangular geometry)
u	laplace space variable
v	velocity, LT^{-1}, ft/min
v_i	interstitial velocity, LT^{-1}, ft/min
$v_{i,opt}$	optimum interstitial velocity, LT^{-1}, cm/min
$v_{i,tip}$	interstitial velocity at the tip of wormholes, LT^{-1}, cm/min
v_{wh}	wormhole propagation rate, LT^{-1}, ft/min
w	fracture width, ft
x_f	fracture-half length, ft.
y_{De}	dimensionless reservoir length (rectangular geometry), ft
y_e	drainage area half-width (rectangular geometry), ft
Z	gas compressibility factor

Greek

α_z	wormhole axial spacing coefficient
γ	specific gravity
Δp_f	frictional pressure drop, $ML^{-1}T^{-2}$, psi

Δp_{PE}	hydrostatic pressure drop, $ML^{-1}T^{-2}$, psi
Δt_{sup}	superposition time function
ε	roughness, dimensionless
λ_{Ac}	dimensionless interporosity parameter
μ	viscosity, $ML^{-1}T^{-1}$, cp
ρ	density, ML^{-3}, g/cm3
ϕ	porosity, fraction
ω	dimensionless storativity ratio

Subscripts

i	initial
f	fracture
m	matrix
f+m	total system (fracture + matrix)
s_c	standard condition
sf	surface

TABLE OF CONTENTS

Page

LIST OF FIGURES

Page

LIST OF TABLES

Page

1. INTRODUCTION

1.1. Research Background

It was estimated that more than 60% of the world's oil and 40% of the world's gas reserves are held in carbonate reservoirs before unconventional reservoir came to commercialization in the past decade. However even though unconventional resource play has produced more and more oil and gas, it is still important and attractive for the remaining reserves from carbonate formations to be produced by cost effective manner in uncertain oil and gas prices. The Middle East, for example, is dominated by carbonate fields, with around 70% of oil and 90% of gas reserves held within these reservoirs. Some shale play such as Eagle Ford and Bakken is actually known as carbonate rich shales. Recent trend shows multi-stage acidizing and acid fracturing in carbonate formations based on the technology applied from shale play has been recognized and some cases have been reported in the literature.

Matrix acidizing (called “matrix” because the injection pressure is below the formation fracture pressure) can be done in either sandstone or carbonate reservoirs, but since these carbonate formations are highly soluble in acid, matrix acid stimulation is used as a cost-effective means to enhance well productivity in carbonate reservoirs. The major goal of acid stimulation under matrix conditions into carbonate formation is to create deep penetrating conductive flow channels known as wormholes that bypass the damaged near-wellbore region where there will be virtually no flow in the low-permeability. Effective

and highly conductive wormhole penetration beyond the damaged zone should result in a smaller pressure drop than in the original undamaged formation. Thus, the post-treatment skin effect could be negative. Actually Furui et al. (2010) showed historical field post-stimulation buildup test data in various carbonate reservoirs in Middle East and North Sea fields, where negative -3 to -4 range of skin factors are commonly achieved, which equivalently means wormhole lengths on the order of 10 to 20 ft. achieved. Very effective acid stimulation is achievable with a certain completion method.

Carbonate acidizing designs usually consist of 15 - 20 %wt. HCl, which causes a high surface reaction rate. It is well known that at a given temperature, the ability of a particular acid to generate wormholes is largely dependent on the acid injection rate. At low injection rates, acid spends rapidly on the face of the core and no wormholes, or only short wormholes form. Since, however, at high injection rates, acid flux at the wormhole is very high, tip splitting and side branching is formed thus wormhole growth rate is inhibited, as a result wormholes have ramified structures. Dominant wormhole pattern is obtained at intermediate injection rates. Enough acid reaches the tip to grow a single wormhole, avoiding excessive side-branching. Compared to the two aforementioned wormhole patterns, the dominant wormhole structure propagates the longest wormhole penetration depth with the least amount of acid injected, which is most desired and efficient injection condition shown in the middle in **Fig. 1**.

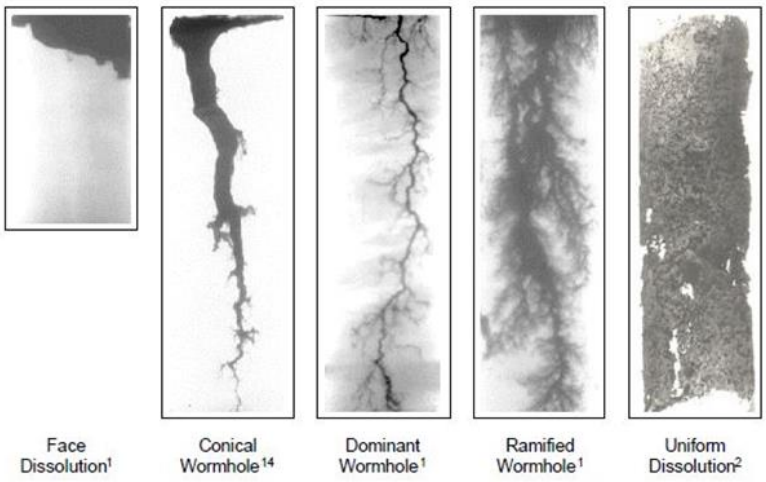

Fig. 1 Wormholes formed by different injection rates (Fredd et. al, 2000)

According to Buijse et al. (2005), under linear core flooding experiment, there exist three regions characterized by a low, optimum and high interstitial velocity on the wormhole efficiency curve. Below the optimal flux, dissolution is mostly confined to the rock face nearest to the acid injection point, and this is called compact dissolution regime, which should be avoided because longer wormholes will not be formed. Above the optimal flux, dissolution occur more side branching and called ramified dissolution regime, which is less efficient compared to the dominant (optimum) wormhole regime. Wormhole efficiency curve generated through laboratory linear-core flooding experiments as shown in **Fig. 2** indicates that there is a certain optimal flux for which wormholes will most efficiently propagate along the main axis of the core plug. The injection rate, at which the dominant wormhole pattern is obtained, is called the optimum injection rate on an acid treatment. For highly reactive acid/rock systems, the optimum injection rate does exist and it depends on the rock mineralogy, acid concentration and reaction temperature and other parameters (Wang et al., 1993).

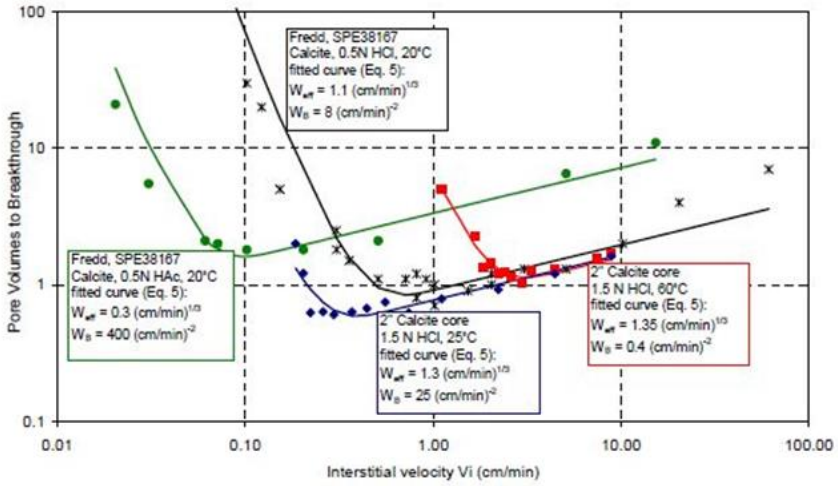

Fig. 2 Wormhole Efficiency Curve (Buijse-Glasbergen, 2005)

Since wormholes are much larger than the pores in non-vuggy carbonates, pressure drop through the region penetrated by wormholes is small and can often be neglected. Thus the wormhole growth is tracked throughout the entire injection period and the stimulation effect contributed by the wormholes is evaluated by a skin factor.

One of the main challenges in predicting the effectiveness of a carbonate stimulation treatment is accounting for the wide range of dissolution structures that can be formed and their impact on skin evolution. Skin varies significantly with dissolution structure due to changes in the depth of penetration (Fredd, 2000). The costs of matrix stimulation treatments depend primarily on the volume of injected acid (which influences treatment time) and the equipment to pump acid into the formation at a certain injection rate thus optimization should be done by maximizing incremental production obtained by a matrix acidizing treatment and to balance with cost (Economides at el, 1994). Recent completion and stimulation methodology for long horizontal wells which are more

complicated, affects completion costs (Jackson, 2012). Limited-entry multi-stage stimulation, pre-perforated liner and isolation packers, acid jetting are the examples. Although selection of acid placement from various scenarios depends on what the goal of treatment is, maximum productivity throughout optimum injection condition in field scale is critical to improve economics.

How to create long wormholes in near-wellbore region through optimum injection condition (least acid volume) has been challenging but it is still an area of extensive study. Among lots of wormhole predicting model presented before, it would be key to cover that a model is simple to apply and allows upscaling from laboratory condition to field scale. Skin evolution in treatment monitoring can be an important source of information that helps us characterize the reservoir and understand wormhole growth thus by changing uncertain parameters, the acidizing forward model used in design phase is able to be history matched with comparing the real-time observation of simulation results. Practical guideline to implement optimum acid treatment should be necessary.

On the other hands, acid fracturing is a stimulation conducted above the closure stress, so that a hydraulic fracture is created. Viscous pad fluid creates an initial crack geometry, which increases the contact of the well with the reservoir. Then viscous acid is injected to dissolve the rock along the faces of the fracture and generate etched width along the fracture. After flushing and injection pressure released, the fracture is allowed to close by the closure stresses in the formation but it does not close completely due to the removal of rock at the fracture surface.

Multi-stage acid fracturing in a tight carbonate formation can be an alternative to propped fracturing as relatively cost-effective stimulation treatment. However the success of treatments depends on many factors as to whether enough conductivity is secured and if the conductivity sustains, the selected treatment works under the in in-situ in a specific geologic environment. Thus, observation and evaluation of past practice is important and inevitable step to improve stimulation desings. In this study, the methodology to conduct performance evaluation of acid fracturing treatment using treatment and production records is described, and a field example is used to illustrate how the procedure works.

Field application of the evaluation procedure shows the effectiveness of the approach. Actual cross-sectional area growth, using the monitoring program, is shown as fracture extension and acid etching during the stimulation, which also can be a validation tool for fracture simulation. With production data analysis, it allows us to compare flowing cross-sectional area with induced area by the treatment therefore treatment efficiency is measured. The suggested approach provides engineers with additional information as to whether the designed acid fracturing was performed appropriately under the in-situ closure stress field. It is eventually helpful to discuss past practice and improve candidate selectivity in a company decision making process.

1.2. Literature Review

Literate review for both matrix acidizing and acid fracturing is conducted from the research perspectives. This literature review summarizes past and current practices and

clarifies what was done before. On the basis of the literature review, the research objectives and approach should be defined in next section.

1.2.1. Matrix Acidizing

The review of matrix acidizing covers laboratory experiment and simulation conducted by both linear and radial flow geometry, field condition and upscaling from laboratory condition, treatment monitoring, history matching, and optimal condition.

1.2.1.1. Treatment Design

For treatment design, literature review is categorized into linear core-flooding experiment and simulation, radial core-flooding experiment and simulation, and field condition and upscaling. Matrix acidizing has been extensively studied under linear core flooding condition experimentally. Under laboratory conditions, acid is injected from one end of a cylindrical core sample at a constant rate and the overall pressure drop is monitored. Generally, HCl acid is injected axially into carbonate core samples with diameters ranging from 1in. and lengths ranging from 1in. to 20 in. Acid is pumped at a constant rate until acid dissolves enough material to break through the opposite end of the core.

1.2.1.1.1. Linear core flooding and simulation

Wang et al. (1993) studied the optimum injection rate in carbonate cores. They found that there exists optimum rate and reaction pattern in high reactive acid, varying with rock mineralogy, acid concentration and reaction temperature. Bazin (2001) that reported optimum injection rate increases with acid concentration, temperature, and limestone

permeability. An increase in temperature, concentration and permeability shifts the optimum flow rate to higher values. The optimum rate became independent of the core length greater than 20 cm when the wormhole develops in the mass-transport-limited regime. It was also confirmed that high injection rates are required to increase wormhole penetration distance thus maximum flow rate provides maximum penetration. Buijse and Glasbergen (2005) showed in the plot of wormhole growth rate, V_{wh} versus interstitial velocity, V_i, where optimum injection rate ($V_{i\text{-}opt}$) associated with the minimum pore volume to breakthough ($PV_{bt\text{-}opt}$, the smallest volume of acid required for wormhole breakthrough) does not imply a maximum wormhole growth rate. Rather Vwh is always an increasing function of V_i, even if V_i is larger than $V_{i\text{-}opt}$ as shown in **Fig. 3**.

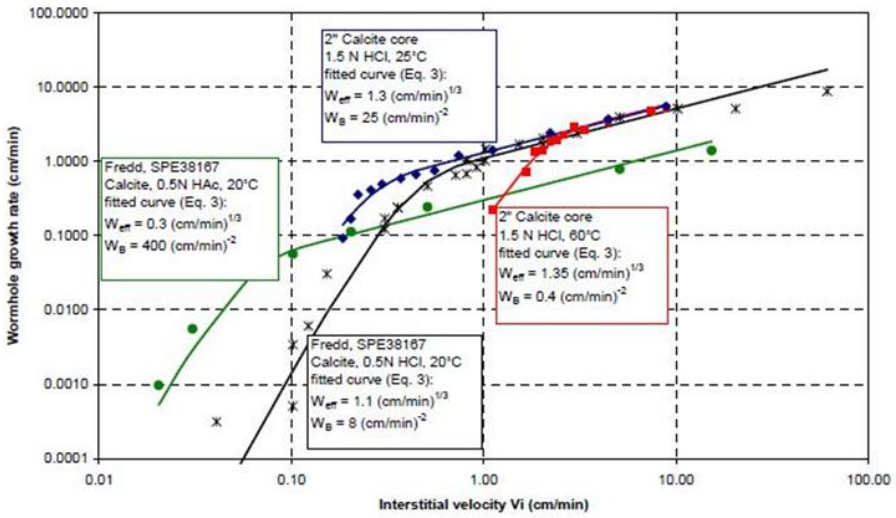

Fig. 3 Wormhole growth rate as a function of injection rate

Cohen et al. (2008) conducted numerical simulation study for different domain (length is equal to 25cm constant, height varying between 5, 10, 20 and 40 cm) and

observed PV_{bt} is in general higher for "confined" conditions (height is equal to 5 and 10 cm) than for "unconfined" domains (height is equal to 40 cm). They found geometry effect can drastically change the dissolution patterns and optimum conditions, and boundaries of the core can greatly disturb the wormholing phenomenon by inhibiting the mechanism of wormhole competition. They demonstrated in the simulation, when shape factor, F (the ratio of the domain height over the domain length, F equal to 1 would define a square domain) is more than 1 (unconfined domain, field scale), the flow rate in the wormhole at optimum conditions becomes independent and stays constant. They concluded experiments done in confined conditions have probably over-estimated the optimum injection velocity and the dissolution dynamic is dependent of the core geometry in unconfined conditions.

Izgec et al. (2008) found that optimal flux in vugular limestone is one to two orders of magnitude lower than that measured with the same acid formulation in homogeneous carbonates through the acidizing process. The experiments were conducted with 4-inch diameter by 20-inch long core samples. This was likely because the acid is flowing through only a small portion of the rock in the vugular limestone case.

Kalia and Balakotaiah (2009) showed from their simulation study that PV_{bt} depends on the aspect ratio at low and intermediate injection rate but is independent of the domain size at high injection rates. They also studied the effect of initial porosity on pattern formation and reported the amount of acid required to break though is higher for higher porosity sample because the amount of leak-off from the channel increases as the local porosity increase. Their study also found that as the heterogeneity magnitude was

increased, PV_{bt} decreases, depending on the presence and the connectivity of vugs. Injection through perforation showed flow expansion in the transverse direction occurs as soon as it enters the medium, which lead to higher PV_{bt} as compared to the regular injection case.

Furui at el. (2010) confirmed the consistent trend from the high porosity outcrop chalk samples that $PV_{bt\text{-}opt}$ values in larger core samples are smaller as shown in **Fig. 4**. In 3D FEM simulation study of comparing 1 in. diameter with 4 in. diameter core effect, the results showed the interstitial velocity at the tip of the wormhole, Vi,tip-opt increases until the wormhole penetration length reaches to core diameter and after reaching the length, the tip velocity of the wormhole becomes relatively constant, which explains why the apparent wormholing efficiency is greater for larger diameter core samples.

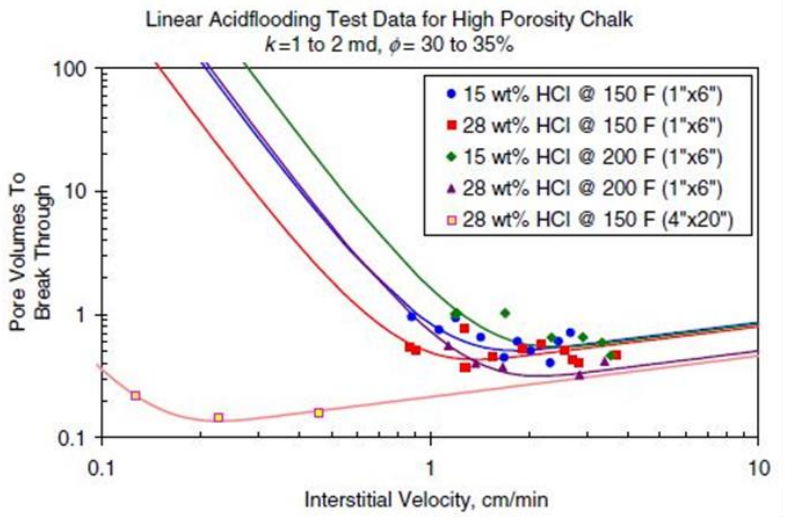

Fig. 4 Linear core flooding experiments of 1" and 4" in. (Furui at el. 2010)

Kai at el. (2013) studied the effects of core length and core diameter on the optimum condition experimentally and found that a stable value of the optimal acid flux

was obtained in 6 inches or longer cores. Because there may be more than one wormhole formed close to the entry, the wormhole competition effect reduces the tip velocity of the wormholes in short core length. However, when the core is long enough, a relatively constant tip velocity of the wormholes can be maintained, and the wormhole propagates more efficiently.

1.2.1.1.2. Radial core flooding and simulation

According to Buijse et al. (2005), the basic physical and chemical principles underlying the wormhole growth process are the same in linear and in radial geometry. However a fundamental difference between linear and radial geometry is the dependence of V_i on position. In linear geometry, V_i is independent of the position in the core and consequently, V_{wh} depends only on the injection rate, and not on the position of the wormhole front in the core. However, in radial geometry, V_i decreases as the distance R from the wellbore increases. Thus longer, deeply penetrating wormholes would receive less acid at the tip, and consequently would grow at a lower rate, compared to short wormholes.

Mostofizadeh and Economides (1994) conducted radial core flood experiments and reported that reaction pattern was consistent with those obtained by linear core-flooding conducted by Wang et al. (1998). However, the pattern are far more complicated and multi-faceted in radial geometry. It was also reported that the optimum acid injection rate depends on the mineralogy and morphology of the reservoir and on the transition point from diffusion-limited to fluid loss-limited modes, which is also related to the acid concentration and temperature. Optimum injection rate highly depends on permeability.

For low permeability rock, optimum injection rate should be lower but rock with increasing permeability would require higher optimum injection rate because the area-to-volume relation increases and the highly unstable nature of the acid attack on the rock is enhanced.

McDuff et al (2010) conducted larger-scale. CT scan image of two experiments conducted at near-optimal rate and at below-optimal rate with Indiana limestone using 15% HCl acid are shown in **Fig. 5** and **Fig. 6**, where the experimental condition corresponds roughly to pumping 40 bpm into 5000 ft. of completion interval and generating 10-25 ft. wormholes into the formation. Nearly four times the acid volume was required in the low-rate condition compare to the near-optimal rate experiments.

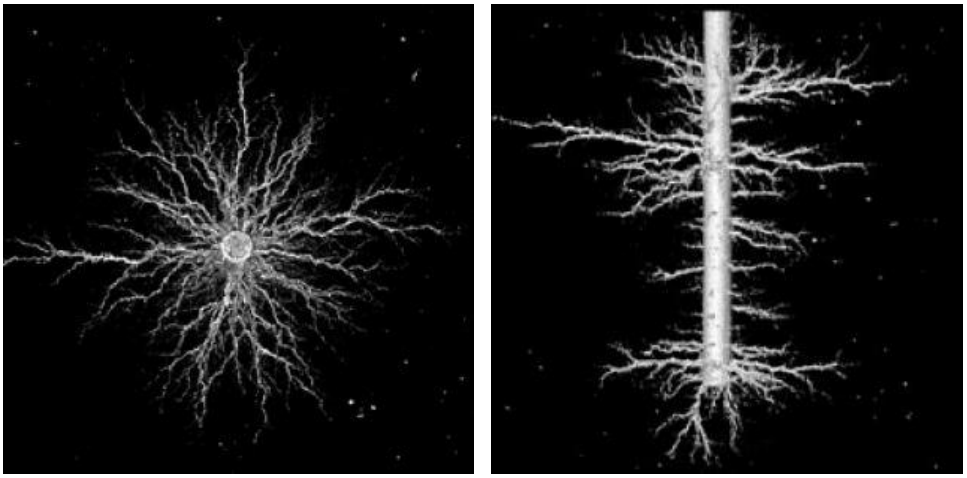

Fig. 5 Top and side views from optimal-rate experiments (McDuff et al. 2010)

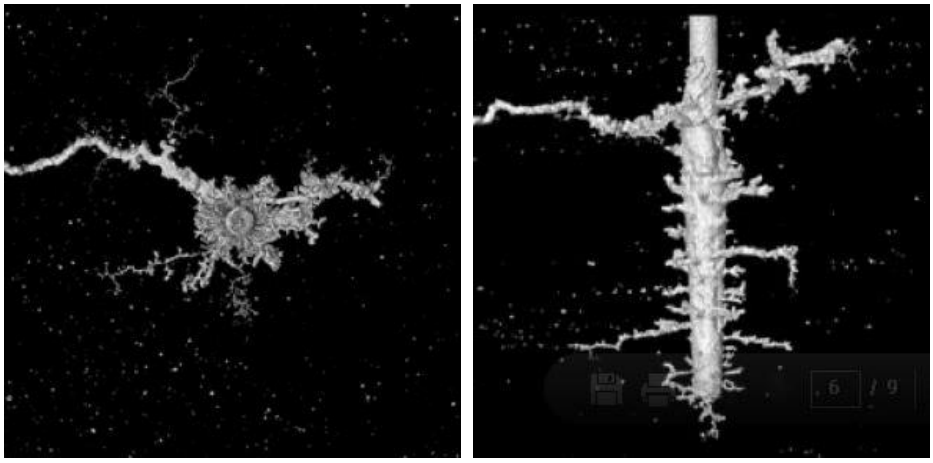

Fig. 6 Top and side views from low-rate experiments (McDuff et al. 2010)

Cohen et al. (2008) conducted numerical simulation study about radial geometry. Their main observation was that dissolution close to the optimum injection velocities is achieved in radial flow at higher injection velocity than in linear flow.

1.2.1.1.3. Field condition and upscaling from lab condition

As evidenced by many researchers describing the optimum injection rate measured in a linear core-flooding experiment cannot be translated easily to field conditions, where flow is very likely to radial flow. In radial geometry, optimal wormhole-growth rate in radial flow does not come from a single pump rate, but changes as the formation is penetrated by the wormhole front. Longer wormholes require a higher pump rate to grow efficiently thus pump schedule should start at relatively low pump rates, and increase the pump rate during the treatment. It actually requires real time knowledge of wormhole growth rate and penetration depth, which is difficult to obtain.

Buijse et al. (2005) and Glasbergen (2009) recommended the best practice is to pump at the maximum rate possible below the fracturing pressure. Glasbergen (2009) reported several other factors will play a role under field conditions. Injection rate limitations because of fracture pressure or equipment limitations, heterogeneities in mineralogy, variations in injection temperature, variations in injection rates including shut-ins, the effect of diverters and wellbore effects such as travel time for the acid from the heel to the toe is the examples.

Furui et al. (2010) developed the modified wormhole growth model based on Buijse and Grasbergen's empirical correlation. The new wormhole model estimates the wormhole evolution with the consideration of acid flux at the tip of the wormhole, overcoming core size dependencies, which allows upscaling from laboratory linear core-flooding on small cores to radial/spherical flow geometries in field-size treatment.

1.2.1.2. Treatment Monitoring

Paccaloni et al. (1988) introduced a method that used instantaneous pressure and rate to calculate skin factor continuously. This method is based on the concept of finite-radius "acid bank" and steady-state, radial Darcy's flow. **Fig. 7** illustrates skin evaluation for the field case using Paccoloni's method.

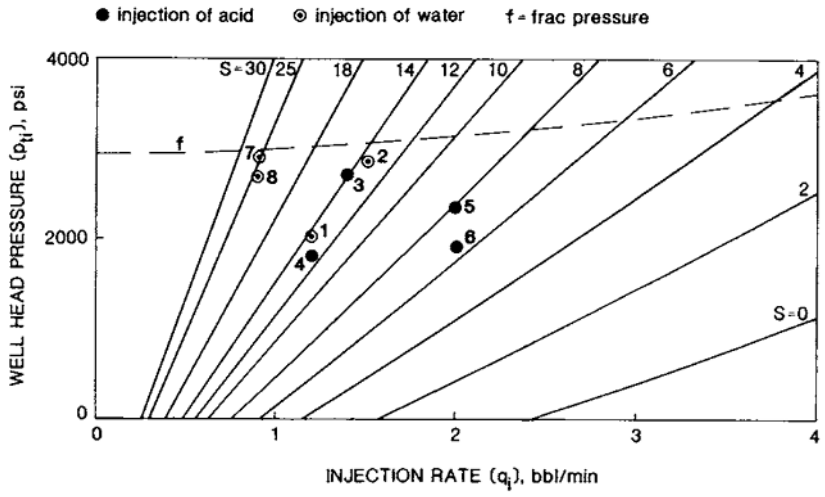

Fig. 7 Field case results (Paccaloni et al., 1988)

Another technique by Prouvost and Economides (1989) proposed to analyze skin evolution by continuous comparison of measured and simulated pressures. The technique requires simulation of the transient pressure response to the injection of inert fluids. The flow rates used for the inert fluids follow the exact injection schedule of the acid treatment. The difference between the actual bottomhole pressure and simulated bottomhole pressure is utilized to evaluate the changing skin factor. Hill and Zhu (1996, 1998) proposed a method based on the theory of standard injectivity test using approximate line source solution for transient flow to monitor changing skin during matrix acidizing treatment (**Fig. 8**). Furthermore, this approach employs a superposition method to account for the transient flow effects due to injection of acid at multiple rates and pressures. Therefore, each point on the inverse injectivity vs. superposition time plot will lie on a straight line having slope, m, with its intercept depending on the skin factor at time t.

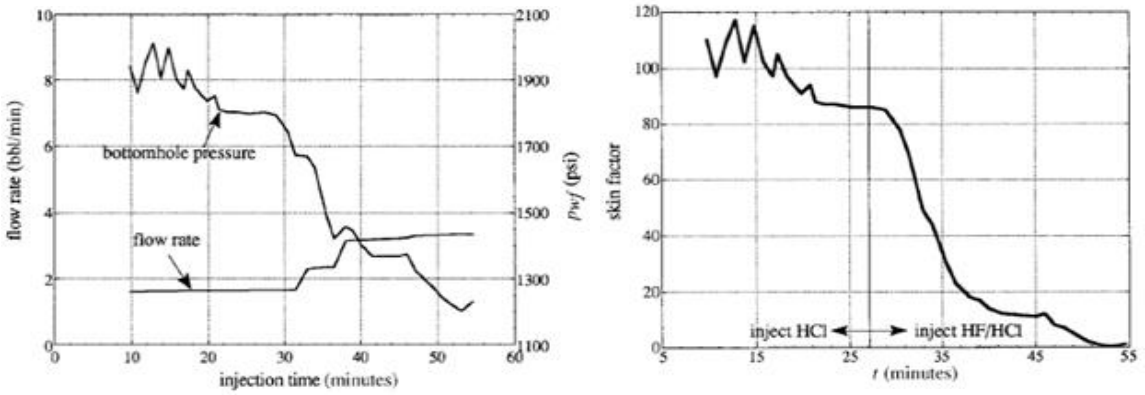

Fig. 8 Field case results (Zhu and Hill, 1998)

For recent practical example, Kent et al.(2014) showed the skin evolution treated by multi-stage intelligent completion. The evolution of effective wellbore radius through the chalk formation in North Sea was monitored during injection. Skin was -4.4 at the end of the treatment, showing a successful stimulation treatment.

1.2.1.3. History Matching

Buijse et al. (2005) conducted a field case study using acid placement model based on their wormhole model. **Fig. 9** shows measured and simulated pressures and skin during the stimulation, having a good agreement.

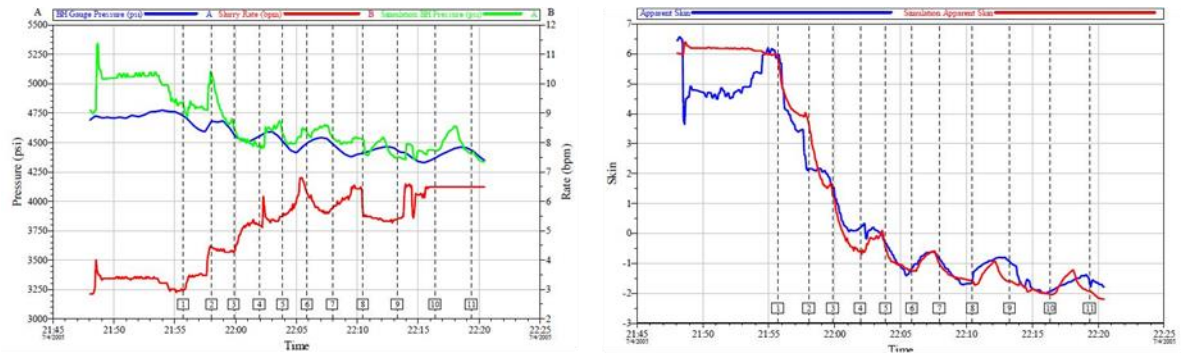

Fig. 9 Pressure and skin evolution match (Buijse et al. 2005)

Varun et al. (2007) conducted pressure history matching using their developed acid placement model. The reservoir permeability and the PV_{bt} in the volumetric model were adjusted to obtain a match of the actual treating pressure. Furui et al. (2010) showed in a case study of downhole injection pressure matching results during an acid injection where measured $PV_{bt,opt}$ and $V_{i,opt}$ were used based on the linear core-flooding experiments. Simulation with conventional radial flow showed the downhole injection pressure becomes too high because $V_{i,tip}$ is lower and calculated wormhole penetration depth is too short. In the upscaling method, the wormholing axial spacing, αz was changed until a good match and final value was αz was 0.75, where dominant wormhole with some spacing allows much higher $V_{i,tip}$ at wormhole tip than conventional radial flow condition.

1.2.1.4. Optimum Condition

Glasbergen et al. (2009) described the constraints of optimum injection rate for wormhole propagation on the basis of excellent literature review and case studies. According to their study, to be a candidate for applying optimum injection rate, the reservoir pressure should be fairly uniform, the total zone height should be relatively short, and no major variations in permeability should be present. Although the optimum injection rate does exist for HCl, it is necessary to know the injection flow distribution. Real-time measurements should help determine the flow distribution and can potentially be used to determine the best flow rate or maximum injection rate. It is recommended to increase flow rate during a treatment and eventually apply maximum available pump rate below fracture pressure in combination with diverters when limited information of reservoir is available or reservoir

pressure variations are expected. Thus application of the flow rate lower than the maximum allowed flow rate can be considered only when (1) the optimum flow rate is fully understood under radial conditions; (2) the flow distribution during a treatment is known at all times; and (3) the theoretical optimum flow rate is significantly lower than the maximum allowed flow rate.

1.2.2. Acid Fracturing

1.2.2.1. Treatment Design and Monitoring

The design of an acid fracturing treatment is accomplished by estimating the optimum conductivity and acid penetration distance that results in maximum benefit of the treatment. Design parameters include selecting the fluid types, number of stages, pumping rate, and injection time. Changing these parameters results in different fracture geometry, etching patterns, and acid-penetration distance. A complete study of fluid properties, mineralogy and permeability distributions, and formation temperature should be conducted prior to the stimulation. Simulators are usually used to estimate how these design parameters affect the stimulation job (Jawad, 2014).

The effects of acid solutions injected into hydraulic fractures created in carbonate formations can be assessed at the laboratory scale in acid fracture conductivity test that mimic the conditions in an actual acid fracture treatment (Pournik, et. al, 2010). **Fig. 10** shows that 3D images of the etching pattern by a certain acid. The etching profile shows the difference between the original surface and after the acid etching process. The etched fracture surface volume was calculated from the difference in surface volume between the

before and after acidizing. From the etched surface volume, the etched surface width is calculated using the cross sectional area of the fracture.

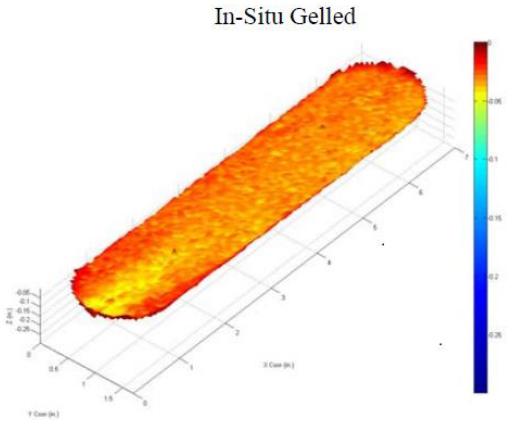

Fig. 10 3-D etched profiles for an acid system (Pournik, et. al, 2010)

1.2.2.2. Production Data Analysis

Evaluations of acid-fracturing treatments are usually based on a production increase or a comparison with other wells. These evaluations determine the relative success of materials and techniques compared with other materials and techniques (Elbel, 1994). The analysis of post-fracture treatment is conducted by pressure-buildup data and/or production data. Production from acid fractures differ significantly from propped fractures. Although created open fractures have an almost infinite conductivity, taking into account in-situ stresses and formation strength affects the post-stimulation performance significantly (Ben-Naceur, Economides, 1989). If etching is non-uniform, the fracture may close with conductivity retained, as depicted in **Fig. 11** (Kalfayan, 2007).

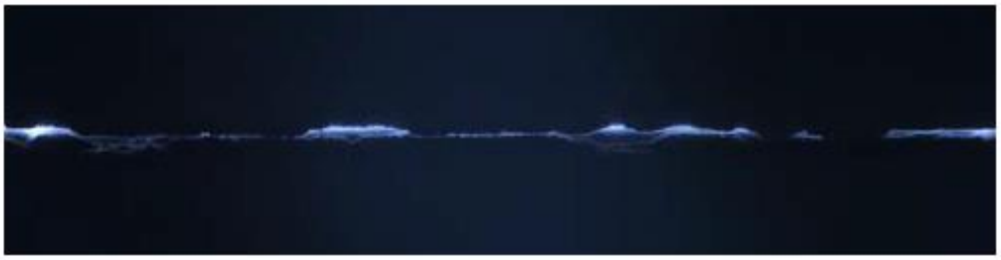

Fig. 11 Backlit acid-etched width from a laboratory core (Kalfayan, 2007)

For flow regime identification, linear flow can be detected by 1/2 slope line in log-log plots of either pressure drop or reciprocal of production rate versus time as shown in **Fig. 12**. Useful plot is the square root of time plot in which Δp or 1/q data is plotted versus. $\sqrt{t}$ as shown in **Fig. 13**. For gas well, pseudo pressure should be used and a straight line of $\Delta m(p)/q_g$ vs. $\sqrt{t}$ plot, either for the constant q_g production or the constant p_{wf} production cases is equivalent to the half-slope period in a log-log diagnostic plot. We can then record the slope of the straight line and the actual time when the boundary is reached. We use the slope of the line and end of half-slope time to calculate$\sqrt{k}A_c$. If matrix permeability is identified, cross-sectional area flowing from fractured wall, A_c can be calculated.

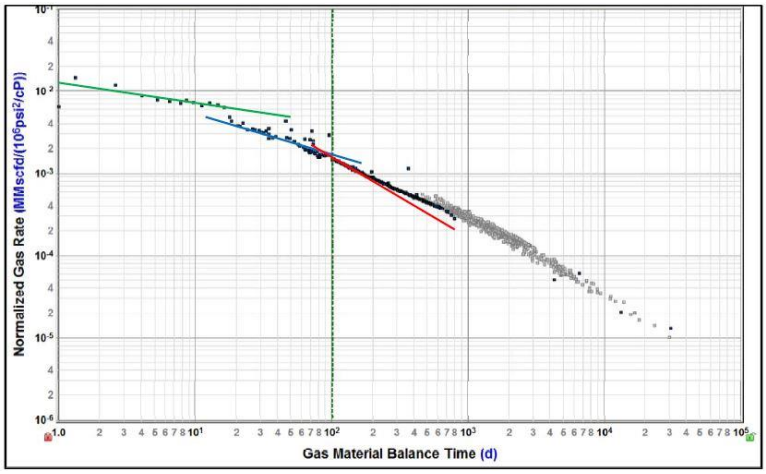

Fig. 12 Flow regime identification (Samandrli et al. 2014)

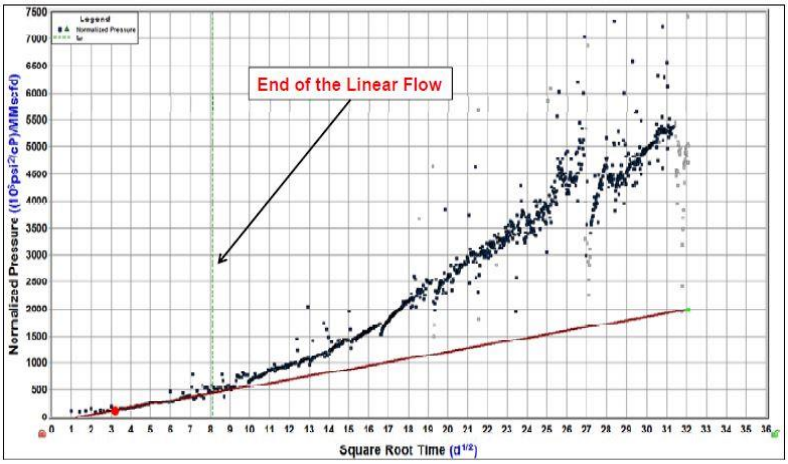

Fig. 13 Square root of time plot (Samandrli et al. 2014)

1.3. Research Objectives

Through the literature review in the previous section, it is clear that how to reduce uncertainty is still the key to achieve optimal treatment. The research goal is to establish

practical guideline to evaluate both matrix acidizing and acid fracturing through integrated approach based on treatment monitoring.

For matrix acidizing, it can be done by combining design, monitoring, history matching as a closed loop. In this study, the latest Furui's augmented wormhole model (2010) on the basis of Buijse and Glasbergen correlation model (2005) is adopted because according to the literature review, Furui's model includes the consideration of acid flux at the tip of the wormhole, overcoming core size dependencies, which allows upscaling from laboratory linear core-flooding to radial/spherical flow geometries in field-size treatment. However uncertain parameters still exist in design phase. Skin evolution available during treatment monitoring is used for history matching process.

For acid fracturing, the method to evaluate acid fracturing is through treatment monitoring and production data analysis. New method for real-time monitoring of acid fracturing, the inverse injectivity vs. superposition time function plot is proposed. By monitoring cross-sectional area from injection flow, real-time area growth induced by acid fracturing is monitored. Comparing the stimulated area with the result from linear flow diagnostic approach from production data, the treatment efficiency can be measured. It provides engineers with additional information as to whether the designed acid fracturing was performed appropriately under the in-situ closure stress field.

In the summary, the goal of this work is divided into two:

1. Matrix Acidizing:

1) To integrate the related models described in the literature. Existent horizontal well acid simulator, Acid Jetting model, and skin monitoring program are consolidated as one integrated tool package.

2) To conduct parameter sensitivity study in order to identify influential parameters in Furui wormhole model.

3) To develop a consistent procedure that can be used from treatment monitoring to history matching so that the result is used to optimum condition study.

2. Acid Fracturing:

1) To develop new monitoring method

2) To develop a consistent procedure that can be used from treatment monitoring to production analysis to measure treatment efficiency.

2. INTEGRATED OPTIMIZATION OF MATRIX ACIDIZING

2.1. Background

In this chapter, all related existent programs and models are integrated to one package for matrix acidizing so that one can use it 1) to design a treatment based on the well structure and completion, 2) to monitor stimulation efficiency during treatment and 3) to conduct history matching the monitored data during treatment and the designed data to update reservoir and key wormholing parameters and 4) to optimize future well stimulation using the updated parameters. This procedure is illustrated in **Fig. 14**.

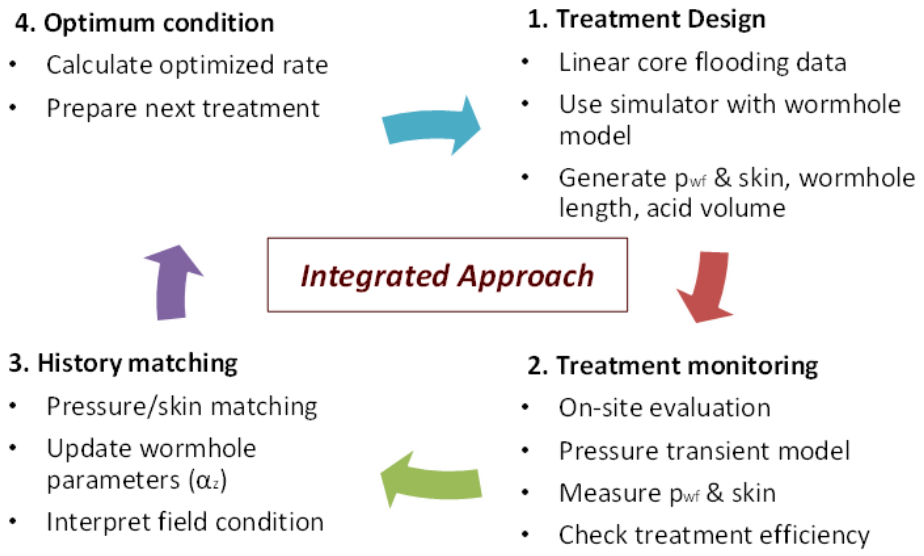

Fig. 14 Integrated approach for optimum matrix acidizing

2.2. Treatment Design

The existing numerical acidizing simulator for horizontal well used in this study was originally developed by the Mishra and Furui (2007). The modification was made by Nozaki (2009) for vertical well in gas reservoir where the viscous diversion effect was included. Tran (2013) added Furui's wormhole model and apparent skin factor model for viscous diversion for radial flow in horizontal well in openhole condition. In this section, further functions have been added to deal with more completion such as acid jetting and limited entry method.

2.2.1. Horizontal Well Acid Simulator (HWAS)

HWAS is an horizontal well acid stimulation simulator. The simulator shown in **Fig. 15** consist of a wellbore flow model, a wellbore fluid interface tracking model, a transient reservoir outflow model, a wormhole growth model and a skin model. The wellbore flow model accounts for pressure drop and material balance inside the wellbore. The fluid interface tracking monitors the interface between the injected fluids in the horizontal wellbore. The transient reservoir flow model captures the transient effect of varying injection rates that are often seen in well test problems. The wormhole model predicts the wormhole penetration in the formation during the entire acid injection period. The apparent skin model accounts for well completions damaged region, wormholes, reservoir mobility and injected fluids mobility. Final skin factor is a function of wormhole penetration depth with the assumption that wormholes extend beyond damage zone at the

end of the treatment (Tran, 2013). More details are found in the literature (Mishra and Furui, 2007, Tran, 2013).

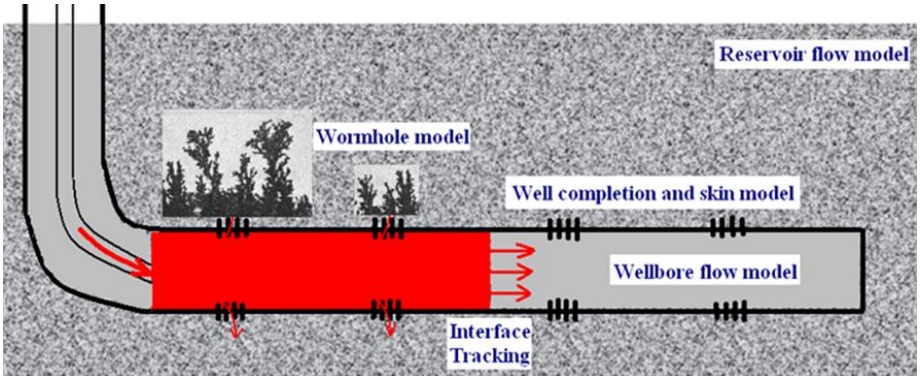

Fig. 15 HWAS model scheme (Wu, 2008)

2.2.2. Integration of Acid Jetting Function into HWAS

Separately, Sasongko (2011) developed an acid placement model by acid jetting out of a drill pipe. Acid is jetted onto the face of openhole wellbore as the drill pipe is withdrawn from the well. The acid is pumped through the nozzle holes giving a jetting effect around the wellbore (**Fig. 16**).

Fig. 16 Acid Jetting Assembly (Sasongko et al. 2011)

The jetting action helps to remove the drilling fluid filter cake and promote the acid to penetrate into the formation and form wormholes to stimulate the well. The model simulates the acid jetting process using a comprehensive model of acid placement and wormhole propagation in a horizontal well. The following steps are taken.

- Openhole horizontal section is divided into a series of segments and each segment represents one cycle of the jetting treatment.
- Mechanical action by acid jetting removes the filter cake around the wellbore section by section. After filter cake is removed, acid goes to the segments and wormhole is created, meanwhile jetting starts to remove the filter cake in the next section as shown in **Fig. 17**.
- The injection acid amounts are controlled by the duration of injection in each cycle, and the pumping rate and the drilling string pulling speed are set close to field operation conditions.

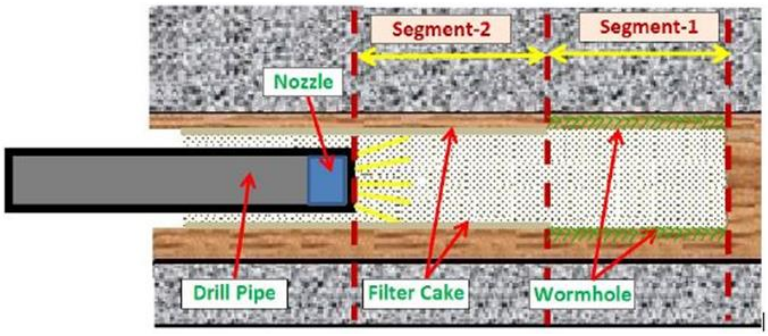

Fig. 17 Filter cake removal in segment 2 and wormhole creation in segment 1

Fig. 18 shows the flow chart with jetting operation. Notice that jetting is an individual module added to tubing location step.

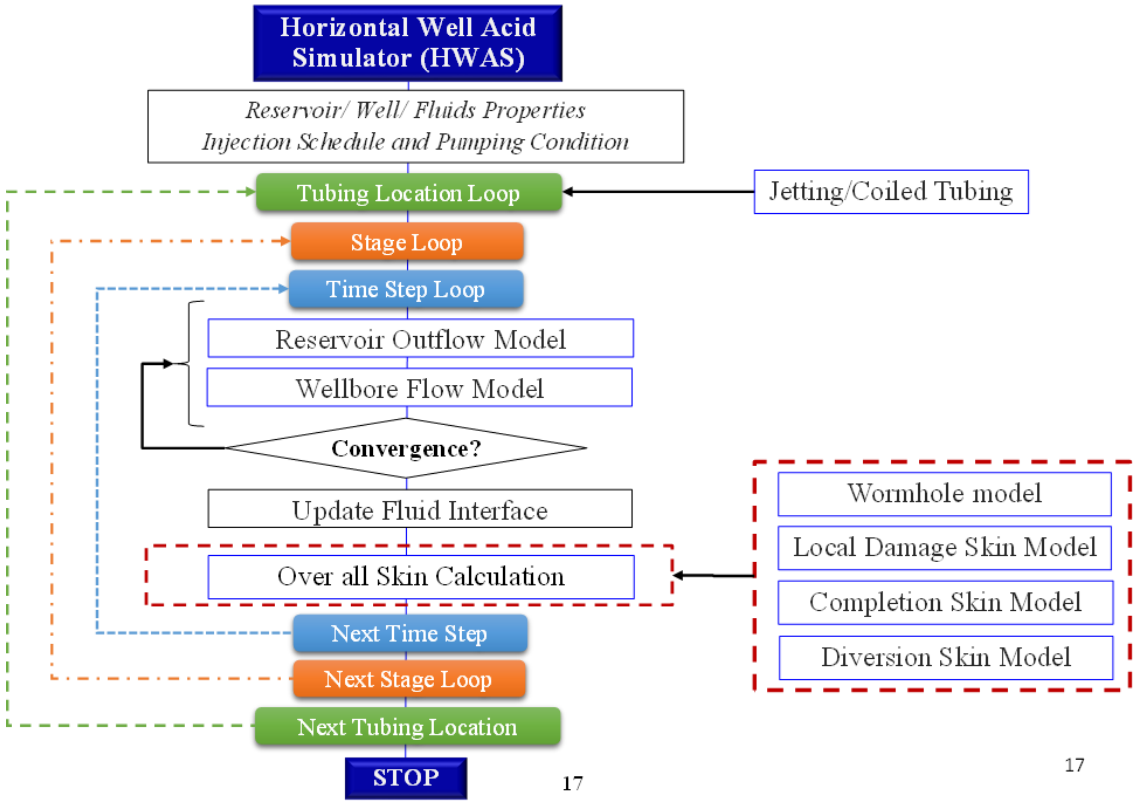

Fig. 18 HWAS flow chart with tubing location loop

2.2.3. Model Validation for Jetting Function

Using same example (Sasongko 2011), integrated jetting function in HWAS was run and validated with the case study result. The input data is shown in **Table 1**. Acid is injected at target volume coverage of 0.5 bbl/ft with a pulling speed of the drill pipe is about 50 ft/min. For the wormhole model, the example case uses a value of 0.53 for optimum pore volume to breakthrough, $PV_{bt\text{-}opt}$, and value of 1.75 cm/min for optimum interstitial velocity, $V_{i\text{-}opt}$. These values were obtained from a laboratory experiment using 1" x 6" core with 15% HCl at 15 °F (Furui et al. 2010).

Table 1 Data input (Sasongko, 2011)

Reservoir & Well Properties	
Parameters	**Input Values**
Avg. Reservoir Pressure	2500 psi
Rock Porosity	31%
Rock Permeability	5 mD
Rock Type	Limestone
Formation Thickness	250 ft
OH Diameter	8.6 in.
TVD/MD	5000/25000 ft.
Openhole Section	20000 ft.
Segment Length	1000 ft.
Filter Cake Thickness	0.1 in.

Stimulation Data	
Parameters	**Input Values**
HCl	15%
Injected Acid Amount	0.5 bbl/ft.
Pumping Rate	20 bpm
Acid Viscosity	1 cp

As the result of the simulation, it was confirmed that the same plot shown in **Fig. 19** was generated compared with the one generated by original acid jetting model. Besides, the simulation time was shrunk dramatically. Compared to 3 minutes running time in original model, integrated function in HWAS took only 5 seconds to finishing calculation. The integrated approach was successfully completed.

According to Sasongko's description, temporarily plugging off the toe end of the well is necessary to increase the flux in the section towards the heel, since the study result shows the toe section is the most stimulated zone and most of the well (up to 75%) receives almost no matrix stimulation other than filter cake removal. Falling to maintain sufficient acid flux into the formation as longer and longer sections are exposed can result in very inefficient matrix stimulation. To maintain wormhole growth throughout such a treatment, the acid flux into the formation cannot drop too far below the optimal flux value.

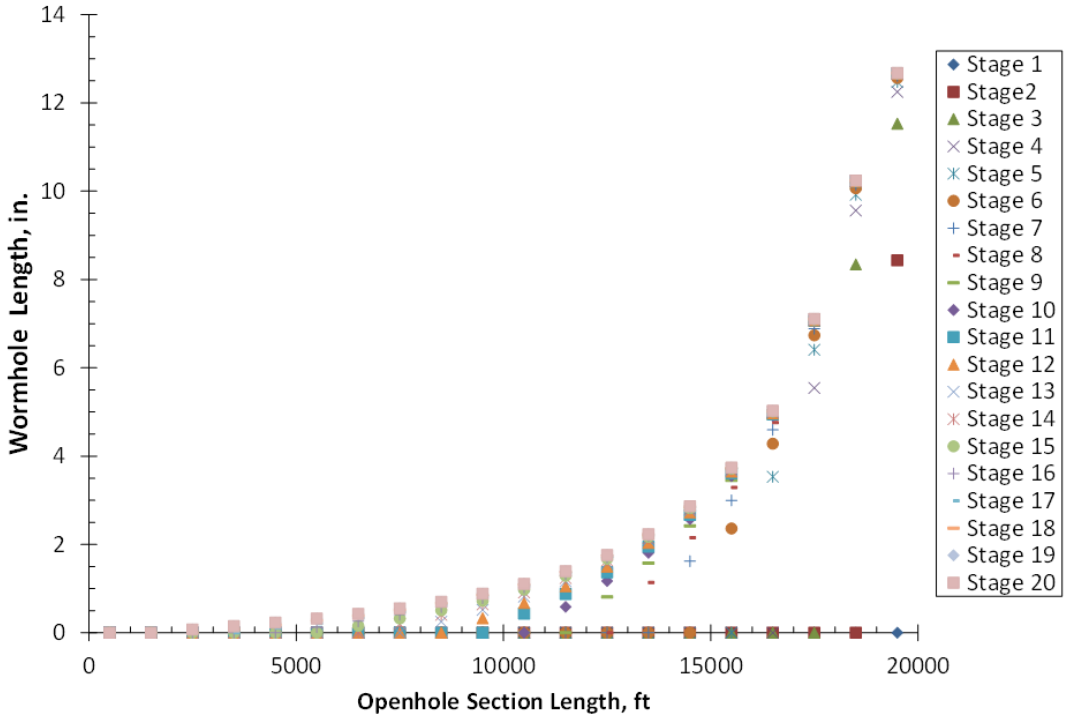

Fig. 19 Wormhole length vs. horizontal section at each treatment

2.2.4. Integration of Limited Entry Function

Limited entry is the process of limiting the number or reducing the entry-hole diameter of perforations in such a way that significant perforation friction pressure is achieved during the treatment. Perforation friction establishes a backpressure in the wellbore that tends to allocate flow among the multiple perforation intervals/clusters, thus improving control of fracturing process. Spherical flow geometry is important for limited entry, especially in the formations in the near-wellbore region until pressure interference among the perforations occurs (Furui at el, 2010). As seen in **Fig. 20**, spherical flow near perforation

region disappears due to no flow boundary at the half-distance between each perforation and the flow pattern approaches to radial flow.

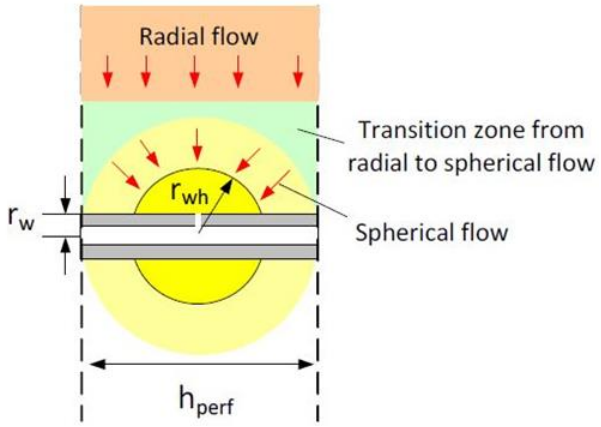

Fig. 20 Spherical flow geometry (Furui at el, 2010)

From program perspectives, the implementation of the transition has been given as follows.

(i) $r_{wh} \le \frac{h_{perf}}{2}$ (Spherical flow)

$$v_{i,tip} = \frac{q}{4\pi\phi d_{e,wh} r_{wh}} \tag{2.1}$$

$$s = \frac{h_{perf}}{2r_{wh}} - \ln\left(\frac{h_{perf}}{2r_{wh}}\right) - 1 \tag{2.2}$$

(ii) $r_{wh} \ge \frac{h_{perf}}{2}$ (Radial flow)

$$v_{i,tip} = \frac{q}{\phi L\sqrt{\pi m_{wh}}}\left[(1-\alpha_Z)\frac{1}{\sqrt{d_{e,wh} r_{wh}}} + \alpha_Z\left(\frac{1}{d_{e,wh}}\right)\right] \tag{2.3}$$

$$s = -\ln\left(\frac{r_{wh}}{r_w}\right) \tag{2.4}$$

2.3. Treatment Monitoring

The concept of inverse injectivity is applied to calculate skin evolution using rate/pressure data during the matrix acidizing treatment. Pandya (2012) developed skin monitoring program in his study. Skin monitoring model has been implemented to HWAS.

2.3.1. Real Time Monitoring During Matrix Acidizing

Hill and Zhu (1996) proposed a method based on the theory of standard injectivity test using approximate line source solution for transient flow to monitor skin during matrix acidizing treatment. The pressure response to multiple injection rates for a vertical well is given by:

$$\frac{p_{wf} - p_i}{q_i} = m\Delta t_{\sup} + b \tag{2.5}$$

where,

$$m = \frac{162.6B\mu}{kh} \tag{2.6}$$

$$b = m\left[\log\left(\frac{k}{\phi\mu c_t r_w^2}\right) - 3.23 + 0.87s\right] \text{ (vertical well)} \tag{2.7}$$

$$\Delta t_{\sup} = \sum_{j=1}^{N} \frac{q_j - q_{j-1}}{q_N} \log\left(t_N - t_{j-1}\right) \tag{2.8}$$

The slope, m, in Eq. (2.6) remains constant as reservoir parameters do not change during acidizing treatment. The only changing parameter is the skin factor, s the equation for

intercept, b Eq. (2.7). Furthermore, this approach employs a superposition method (Eq. (2.8) (Earlougher, 1977)). Using Eq. (2.6) through Eq. (2.8), skin factor can be calculated in real-time from measured pressure, injection rate, and time during an acid treatment from the equation given below:

$$s = \frac{1}{0.868}\left(\frac{b}{m} - \log\left(\frac{k}{\phi\mu c_t r_w^2}\right) + 3.23\right) \tag{2.9}$$

2.3.2. Integration of Power-Law Fluid Function

In order to use the concept of inverse injectivity, it is required to calculate bottomhole pressure. In most acid treatments, bottomhole pressure is not measured and only surface pressure is recorded at the injection tubing or the annulus. **Fig. 21** shows the schematic of the system used for the calculation of bottomhole pressure.

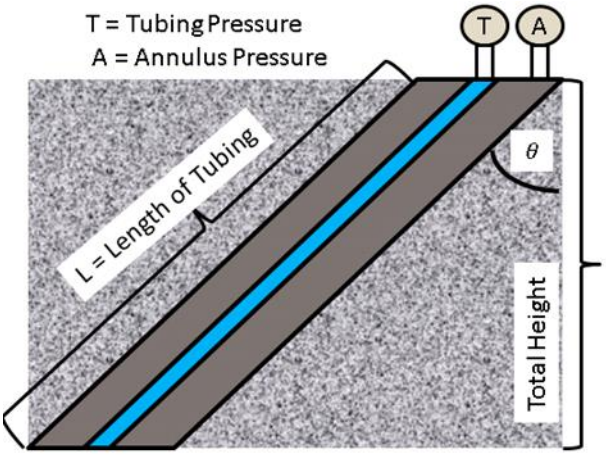

Fig. 21 Schematic of the system for the bottomhole pressure calculation

In the system, the surface pressure can be converted to the bottomhole pressure by

$$p_{wf} = p_{sf} + \Delta p_{PE} - \Delta p_f \tag{2.10}$$

where, p_{sf} is the surface pressure, p_{wf} is the bottomhole flowing pressure, Δp_{PE} is the hydrostatic pressure drop, and Δp_f is the frictional pressure drop. In case the surface pressure is measured in the annulus of the well, the frictional pressure drop is zero and only hydrostatic pressure drop is used to calculate the bottomhole pressure.

For single phase liquid, the hydrostatic pressure drop depends only on the density of the fluid and the height of the fluid column. Therefore, the hydrostatic pressure drop changes when a fluid with different density is injected into the tubing. The hydrostatic pressure drop can be calculated by

$$\Delta p_{PE} = \frac{g\cos\theta}{g_c A}\sum_{i=1}^{N}[\rho_i(V_i - q\Delta t_{new})] \tag{2.11}$$

where, A is the cross-sectional area of the tubing, q is the injection rate, θ is the average inclination of the tubing, ρi-1 is the density of the fluid in the tubing, ρi is the density of the fluid being pumped, Vi is the cumulative injected volume of the i-th fluid, L is the height of fluid of the tubing, and Δt_{new} is the time increment after start of pumping the new fluid.

Considering viscous acid is used, the power-law fluid should be added to the program. Basically the frictional pressure drop depends on the injection rate, fluid density, and fluid viscosity, which may vary during an acid treatment. The friction pressure drop is determined from the Fanning equation,

$$\Delta P_f = \frac{2 f_f \rho\left(\frac{q}{A}\right)^2 L}{g_c D} \tag{2.12}$$

where, f_f is the Fanning friction factor, and D is the diameter of the tubing, In the above equation, the Fanning friction factor depends on the Reynolds number and is explicitly calculated by (Chen, 1979)

$$\frac{1}{f_f} = \frac{16}{N_{RE}} \text{ if } N_{RE} < 2000 \tag{2.13}$$

$$\frac{1}{\sqrt{f_f}} = -4\log\left\{\frac{\varepsilon}{3.7065} - \frac{5.0452}{N_{RE}}\log\left[\frac{\varepsilon^{1.1098}}{2.8257} + \left(\frac{7.149}{N_{RE}}\right)^{0.8981}\right]\right\} \text{ if } N_{RE} > 2000 \tag{2.14}$$

For Power-law fluid, Metzner-Reed generalized Reynolds number equation is used in oilfield units as follows:

$$N_{\mathrm{Re}} = \frac{0.249\rho u^{2-n'} D^{n'}}{96^{n'} K'\left[\left(3n' + 1\right)/ 4n'\right]^{n'}} \tag{2.15}$$

The function of selecting "Power-law" fluid and "K' & n' " in addition to Newtonian fluid was added to the program to calculate bottomhole pressure from surface pressure in viscous fluid.

2.3.3. Integration of Gas Reservoir Function

Fig. 22 shows the schematic of the system for the skin model for horizontal gas well. The system consists of a horizontal wellbore that is bounded in x-direction and z-direction. However, the system is not bounded in the y-direction. Therefore, Goode and Thambynayagam (1987) referred to this model as the semi-infinite slab model.

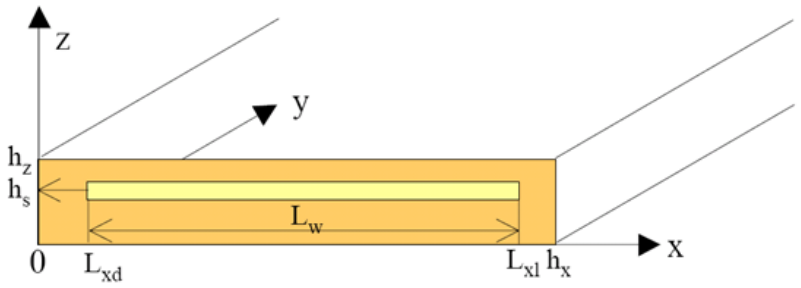

Fig. 22 Schematic for the horizontal well skin model (Zhu et al., 1999)

As for gas reservoir, semi-slab model has been modified for gas case as follows using gas dimensionless pseudo pressure:

$$m_D = \frac{khT_{sc}}{50{,}300qp_{sc}T}(m_i - m) \tag{2.17}$$

In injection, since pressure range is normally more than 3,000 psi, the pseudo pressure can be converted into single pressure:

$$p_D = \frac{khT_{sc}}{50{,}300qp_{sc}T}(p_i - p)\left(\frac{2p_i}{\mu_i Z_i}\right) \tag{2.18}$$

Now superposition time function is written as usual:

$$\Delta t_{\sup} = \sum_{j=1}^{N} \frac{q_j - q_{j-1}}{q_N}\sqrt{\pi\left(t_{D,N} - t_{D,j-1}\right)} \tag{2.19}$$

Since intercept b is obtained in pressure and time monitoring:

$$b = \frac{p_{wf} - p_i}{q_i} - m \cdot \Delta t_{\sup} \tag{2.20}$$

Slope m and intercept b is defined:

$$m = \frac{2 \times 50{,}300 p_{sc} T \mu_i Z_i r_w'}{2 p_i T_{sc} h_x h_z k_y} \tag{2.21}$$

$$b = m\frac{h_x^2}{\pi^2 v_x}\sum_{j=1}^{N}\frac{q_j - q_{j-1}}{q_N}\Pi + m\frac{hxh_z}{L_w v_z \pi}\sum_{j=1}^{N}\frac{q_j - q_{j-1}}{q_N}\Gamma + \frac{50{,}300 p_{sc} T \mu_i Z_i}{2 p_i T_{sc}}\frac{1}{\sqrt{k_y k_z} L_w}s \quad (2.22)$$

The remaining parameters used in Eq. (2.22) are defined:

$$\Pi = \sum_{n=1}^{\infty}\left[\frac{1}{n} erf\left(v_x \pi n\sqrt{t_D - t_{D,j-1}}\right)\Xi_n^2\right] \quad (2.23)$$

$$\Gamma = \sum_{l=1}^{\infty}\left[\frac{1}{m} erf\left(v_z \pi l\sqrt{t_D - t_{D,j-1}}\right)\Xi_l \cos\left(l\pi z_e\right)\right] \quad (2.24)$$

$$\Xi_n = \frac{1}{nL_w}\left[\sin\left(\frac{n\pi L_{xl}}{h_x}\right) - \sin\left(\frac{n\pi L_{xd}}{h_x}\right)\right] \quad (2.25)$$

$$\Xi_l = \frac{1}{4lr_w'}\left[\sin\left(\frac{l\pi}{h_z}\left(h_s + 2r_w'\right)\right) - \sin\left(\frac{l\pi}{h_z}\left(h_s - 2r_w'\right)\right)\right] \quad (2.26)$$

$$z_e = \frac{1}{h_z}\left(h_s + 1.47 r_w'\right) \quad (2.27)$$

$$t_D = \frac{0.000264 k_y t}{\phi \mu c_t r_w'} \quad (2.28)$$

$$v_x = \frac{r_w'}{h_x}\sqrt{\frac{k_x}{k_y}} \quad (2.29)$$

$$v_z = \frac{r_w'}{h_z}\sqrt{\frac{k_z}{k_y}} \quad (2.30)$$

$$L_w = \left(L_{xl} - L_{xd}\right) \quad (2.31)$$

$$r_w' = r_w\left(\frac{k_z}{k_y}\right)^{1/4} \quad (2.32)$$

Finally, skin evolution is given as below:

$$s = \frac{2 p_i T_{sc}\sqrt{k_y k_z} L_w}{50{,}300 p_{sc} T \mu_i Z_i}\left\{b - m\frac{h_x^2}{\pi^2 v_x}\sum_{j=1}^{N}\frac{q_j - q_{j-1}}{q_N}\Pi - m\frac{hxh_z}{L_w v_z \pi}\sum_{j=1}^{N}\frac{q_j - q_{j-1}}{q_N}\Gamma\right\} \quad (2.33)$$

In the above equations, the geometry functions and dimensionless groups are as follows. The infinite summation terms are approximated by the first 40 terms for a stable result. The drawback of this skin model is that it does not consider the effect of reservoir heterogeneity. The variation in permeability and skin along the horizontal wellbore is interpreted using three constant values of permeability (k_x, k_y, and k_z) and one skin value. Thus, the horizontal skin model provides a global estimate of skin evolution and will not provide the skin profile along the horizontal length.

2.3.4. Case Study

Limited entry case study is shown using same input as Furui et al (2010) and the actual skin evolution has been generated. Given input parameters are shown in **Table 2**.

Table 2 Input data (SPE 134265, Furui at el.)

Well & Stimulation Data	
Parameters	**Input Values**
Stimulation length, ft (Stage1)	970
Perforation diameter (in)	0.21
Perforation shot density (SPF)	0.1
Perforation interval (ft)	10
Top perf depth (ft) –MD / TVD	15,173 / 9,632
Acid concentration (wt%)	28
Acid volume (bbl /ft)	1.65

In this case, bottomhole pressure were recorded by the downhole gauge. Since reservoir face pressure is necessary to conduct skin calculation appropriately, hydrostatic, frictional

and perforation frictional pressure drop has been subtracted from the measure pressure (**Fig. 23**).

$$p_{resevoir} = p_{gauge} + \Delta p_{PE} - \Delta p_{f\_pipe} - \Delta p_{f\_perf} \tag{2.34}$$

$$\Delta p_{f\_perf} = \frac{1.98244 q^2 \gamma}{N_{Perf}^2 K_d^2 d_{Perf}^4} \tag{2.35}$$

where, q is the injection rate in bpm, γ is the fluid specific gravity, N_{perf} is the number of perforations, K_d is the discharge coefficient, d_{perf} is the diameter of the openings in inch. Usually the value of K_d between 0.6 and 0.8 is used.

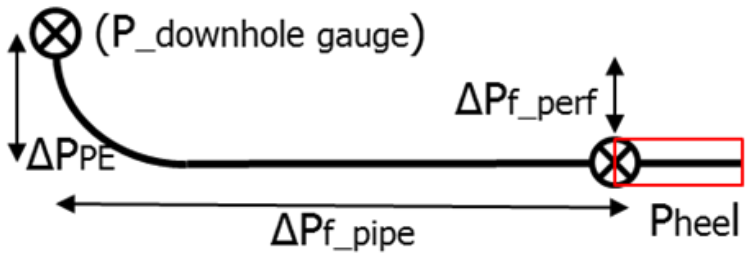

Fig. 23 System schematic of Eq. (2.34)

With fitted friction reducer multiplier, calculated reservoir face pressure is shown in **Fig. 24**. When the reservoir face pressure drop below closure pressure, matrix acidizing occurs.

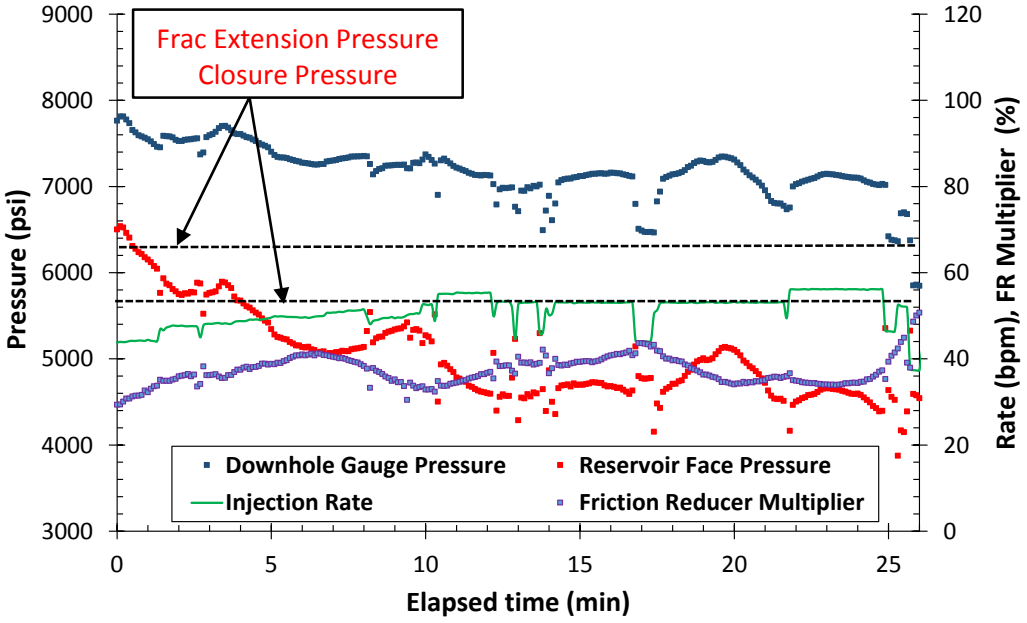

Fig. 24 Reservoir face pressure with time

With reservoir face pressure estimated, skin evolution is calculated. The result is shown in **Fig. 25**. Because the reservoir was hydraulically fractured in the beginning the treatment, initial skin was started by a negative value. Considering limited entry completion, early flow regime is spherical flow but the effect should be dissipated after created wormhole length is extended more than 5ft (the half of the perforation spacing). In this case, around 3 minutes are identified as transition point from spherical flow to radial flow since -3.0 skin is equivalent to 5ft wormhole radius. The wormhole continue to extend in the radial flow condition and the final obtained skin was -4.5 which is equivalent to 20ft wormhole length created by matrix acidizing. Through this case study, the program successfully follows the limited entry case and generate reasonable skin evolution result.

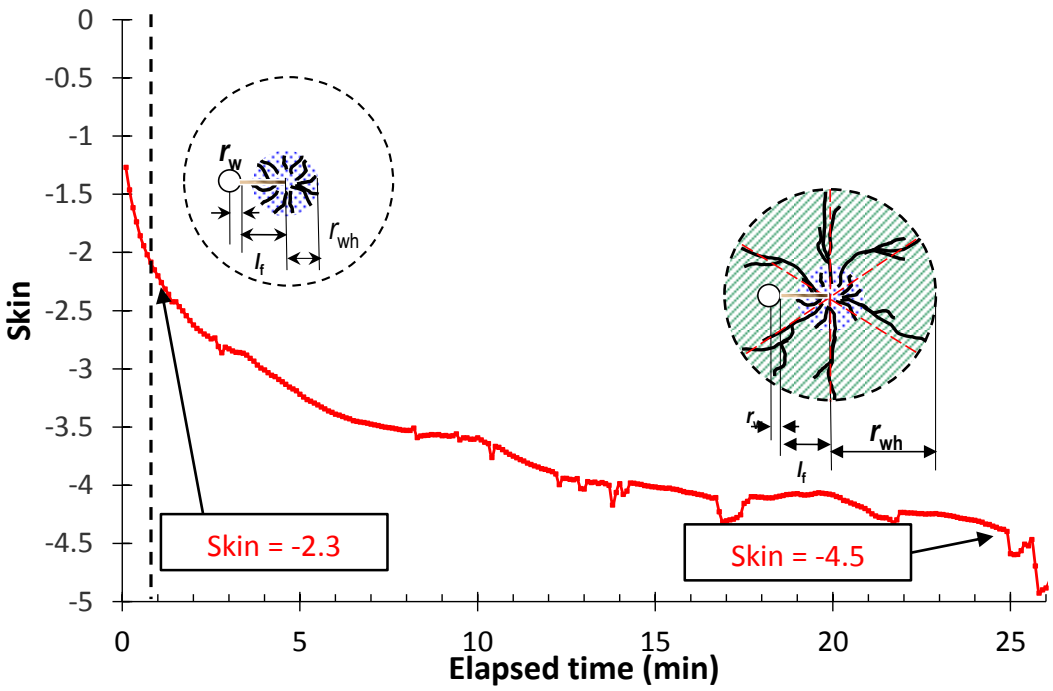

Fig. 25 Skin evolution diagnostic plot

On-site monitoring by skin evolution to evaluate treatment efficiency has been successfully used during stimulation, which can be an important information that helps us to characterize the reservoir and understand wormhole growth. Through history matching process described in next section, uncertain parameters used in the well placement simulator with a wormhole model is able to be modified by comparing the real-time observation with the simulation results.

2.4. History Matching

Now that actual and simulated pressure and skin with time is obtained, next is to history match the two sets of data to evaluate the influential parameters. **Table 3** shows the influential parameters list used in Furui wormhole model.

Table 3 Influential parameter list for history matching

Reservoir & Near-Wellbore	Stimulation / Wormhole
• Porosity, ϕ • Horizontal Permeability, k_H • Permeability Impairment ratio, k_S/k • Permeability Ratio, k_H/k_V • Damage Penetration Radius, r_d	• Optimum Pore Volume to Breakthrough, $PV_{bt\text{-}opt}$ • Optimum Interstitial velocity, $V_{i\text{-}opt}$ • Effective wormhole diameter, $d_{e,wh}$ • No. of Dominant Wormholes, m_{wh} • Wormhole axial-spacing coefficient, α_z

First of all, we need to reduce the number of parameters in the list. Formation evaluation technique by well-logging analysis and pressure fall-off test are highly recommended to obtain the best-estimated reservoir and near-wellbore parameters such as porosity, permeability, damaged zone radius and permeability before designing an acid treatment. Well completion also matters. Although the flow is converged to radial flow at some point, whether the well is perforated and/or fractured before matrix acidizing may give different flow regime rather than radial flow during the early time of acid treatment.

In this study, a sensitivity study using Furui wormhole model was conducted for reservoir and near-wellbore parameters as wells as the wormhole model parameters. The understating of each parameter's effect on pressure and skin evolution behavior during acid stimulation is crucial to further optimization study.

2.4.1. Sensitivity Study

Through the sensitivity study, the influential parameter and physical meaning of Furui wormhole model on the bottomhole pressure and damaged skin versus time is described.

Economides et al. (1994) conducted parametric studies on the post-treatment skin effect. The impact of various factors on the skin effect, including acid volume, ratio of undamaged to damaged permeability, porosity of the original formation, fractal dimension, and injection rate was plotted using their wormhole model (**Fig. 26**).

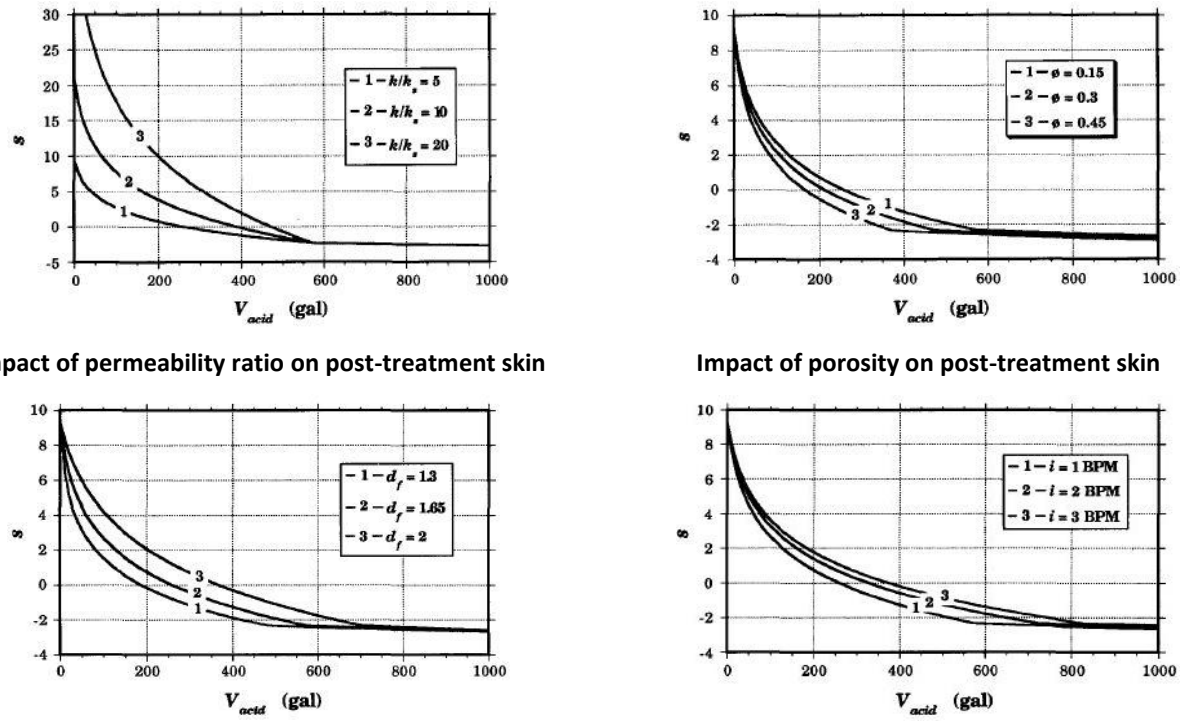

Impact of permeability ratio on post-treatment skin **Impact of porosity on post-treatment skin**

Impact of the fractal dimension on post-treatment skin **Impact of acid injection rate on post-treatment skin**

Fig. 26 Parametric study on the post-treatment skin effect (Frick et al. 1994)

Following the literature, the parametric study conducted in this section plots the impact of various factors on the skin evolution as well as bottomhole pressure over the treatment time, using Furui wormhole model. **Table 4** is the parameter list used in HWAS including both Buijse-Glasbergen model and Furui wormhole model. It is recognized that 3 more parameters are used in Furui wormhole model.

Table 4 Influential parameter list (Buijse-Glasbergen and Furui model)

Buijse-Glasbergen Model	Furui Model
[Reservoir & Wellbore] • Porosity, ϕ • Horizontal Permeability, k_H • Permeability Impairment ratio, k_S/k • Permeability Ratio, k_H/k_V • Damage Penetration Radius, r_d **[Stimulation / Wormhole]** • Optimum Pore Volume to Breakthrough, $PV_{bt\text{-}opt}$ • Optimum Interstitial velocity, $V_{i\text{-}opt}$	**[Reservoir & Wellbore]** • Porosity, ϕ • Horizontal Permeability, k_H • Permeability Impairment ratio, k_S/k • Permeability Ratio, k_H/k_V • Damage Penetration Radius, r_d **[Stimulation / Wormhole]** • Optimum Pore Volume to Breakthrough, $PV_{bt\text{-}opt}$ • Optimum Interstitial velocity, $V_{i\text{-}opt}$ • Effective wormhole diameter, $d_{e,wh}$ • No. of Dominant Wormholes, m_{wh} • Wormhole axial-spacing coefficient, α_z

In this sensitivity study, synthetic horizontal well in a homogeneous limestone reservoir under openhole and radial flow geometry condition (**Table 5**) is used. Each parameter is varied with 3 values, low, mid, and high. Simulation using HWAS and Furui wormhole model is performed repeatedly with no change to the other parameters in order to quantify the sensitivity to the parameter changed.

Table 5 Input data of synthetic well

Summary of Well and Stimulation Data	
Parameters	**Input Values**
Initial Reservoir Pressure (psi)	3000
Fluid Viscosity (cP)	0.50
Formation Thickness (ft)	150
Total Compressibility (1/psi)	3.50E-06
Stimulation Length (ft)	1000
Wellbore Radius (ft)	0.328
Tubing OD (in.)	3.00
True Vertical Depth (ft)	7000
Acid Concentration (wt%)	15
Acid Volume (bbl/ft)	0.6
Injection Rate (bpm)	20

Table 6 Parameter set-up for sensitivity analysis

Base values of each parameters					
Parameter	**Low**	**-**	**Base Values**	**-**	**High**
Porosity, ϕ	0.05	-	0.15	-	0.3
Horizontal Permeability, k_H (md)	12	-	15	-	18
Permeability Impairment ratio, k_S/k	0.2	-	0.3	-	0.4
Permeability Ratio, k_H/k_V	5	-	10	-	15
Damage Penetration Radius, r_d (ft.)	0.5	-	1.0	-	2.0
Optimum Pore Volume to Breakthrough, $PV_{bt\text{-}opt}$	0.45	-	0.85	-	1.25
Optimum interstitial velocity, $V_{i\text{-}opt}$ (cm/min)	0.5	-	1.0	-	1.5
Effective wormhole diameter, $d_{e,wh}$ (in.)	0.1	-	0.25	-	0.5
No. of Dominant Wormholes, m_{wh}	3	-	6	-	12
Wormhole axial-spacing coefficient, α_z	0	-	0.5	-	1

2.4.1.1. Reservoir And Near-Wellbore Parametric Sensitivity Study

The results of pressure-dependent sensitivity for reservoir and near-wellbore parameters are summarized in **Fig. 28**. It is observed that formation damage related parameter such

as permeability impairment ratio (ks/k) and damage radius (rd) are sensitive during early injection time until wormhole radius exceeds damaged zone. As an overall trend, porosity, horizontal permeability and permeability ratio (k_h/k_v) are sensitive during entire stimulation period.

On the other hand, skin sensitivity for reservoir and near-wellbore parameters are shown in **Fig. 29**. It is observed that the overall behavior of skin sensitivity is same as pressure sensitivity. Because the nature of skin is an additional pressure drop in radial flow condition to count for production efficiency deviated from the ideal condition (Furui at el 2003), it is not surprising the parameters affect pressure and skin in a similar trend. However horizontal permeability and permeability ratio (k_h/k_v) are not sensitive parameter because of the way that skin is calculated. The description of each parameter effect on pressure and skin is as follows.

(a) Porosity:

With the superposition principle, the reservoir flow estimation to include the transient effects during acid injection process can be estimated from Lee et al. (2003);

$$-\frac{2\pi kl}{\mu}(p_R - p_w) = \sum_{j=1}^{n} \Delta q_j \left[p_D(t_n - t_{j-1})_D\right] + q_n s_n \tag{2.36}$$

where,

$$\Delta q_j = q_j - q_{j-1_n} \tag{2.37}$$

$$t_D = \frac{4.395\times10^{-6} kt}{\phi\mu c_t r_w^{\ 2}} \tag{2.38}$$

$$p_D \approx \frac{1}{2}(\ln t_D + 0.80907) \tag{2.39}$$

In HWAS, reservoir flow rate and pressure at each time step in radial geometry is solved simultaneously because wellbore material balance is coupled with reservoir flow model. Eq. (2.36), (2.38) and (2.39) indicates wellbore pressure decreases as porosity increases for injection. Skin deceases because of pressure drop. However, in the wormhole velocity described in radial geometry in Eq. (2.40) and (2.41) in Furui's model, $V_{i,tip}$ decreases, resulting in a slower V_{wh} and skin reduction as porosity becomes larger. Thus the difference of 3 cases are minimal.

$$v_{i,tip} = \frac{q}{\phi L\sqrt{\pi m_{wh}}}\left[(1-\alpha_Z)\frac{1}{\sqrt{d_{e,wh}r_{wh}}} + \alpha_Z\left(\frac{1}{d_{e,wh}}\right)\right] \tag{2.40}$$

$$v_{wh} = v_{i,tip}N_{AC}\left(\frac{v_{i,tip}PV_{bt,opt}N_{AC}}{v_{i,opt}}\right)^{-\gamma} \times\left\{1-\exp\left[-4\left(\frac{v_{i,tip}PV_{bt,opt}N_{AC}L_{core}}{v_{i,opt}r_{wh}}\right)^2\right]\right\}^2 \tag{2.41}$$

(b) Horizontal permeability:

Transient reservoir flow in Equation (2.36) shows drawdown is lower as permeability increases. Because permeability effect is included in $PV_{bt,opt}$ and interstitial velocity measured in linear core flooding experiment, wormhole velocity does not change if permeability changes in HWAS thus skin is not changeable.

(c) Permeability ratio:

The distribution of damage around a horizontal well is likely to be highly non-uniform and reservoir anisotropy may lead to an elliptically shaped damage zone perpendicular to

the well, depending on the ratio of the vertical to horizontal permeability (Furui et al. 2002). I_{ani} is the index of anisotropy defined by permeability ratio as:

$$I_{ani} = \sqrt{k_h / k_v} \tag{2.42}$$

Overall skin factor (Furui et al., 2003) over the horizontal lengths is given as:

$$s_{eq} = \frac{L}{\int_0^L \left\{ \ln\left[\frac{I_{ani} h}{r_w (I_{ani} + 1)} \right] + s(x) \right\}^{-1}} - \ln\left[\frac{I_{ani} h}{r_w (I_{ani} + 1)} \right] \tag{2.43}$$

As anisotropy is higher, equivalent skin generates higher thus the bottomhole pressure is calculated higher. For skin calculation, skin govern by wormhole radius thus this effect is not included.

(d) Permeability impairment ratio (k_s/k):

If the wormhole region is still inside the damaged zone, damage skin impacts the flow. After penetrating outside the damage zone, skin factor become negative. (**Fig. 27**).

For $r_{wh}<r_d$:

$$s(x) = \frac{k}{k_d(x)} \ln\left(\frac{r_d(x)}{r_{wh}(x)} \right) - \ln\left(\frac{r_d(x)}{r_w} \right) \tag{2.44}$$

And for $r_{wh}>r_d$:

$$s(x) = -\ln\left(\frac{r_{wh}(x)}{r_w} \right) \tag{2.45}$$

where r_{wh} is radius of region penetrated by wormholes at that particular point, which is to be calculated from the wormhole model.

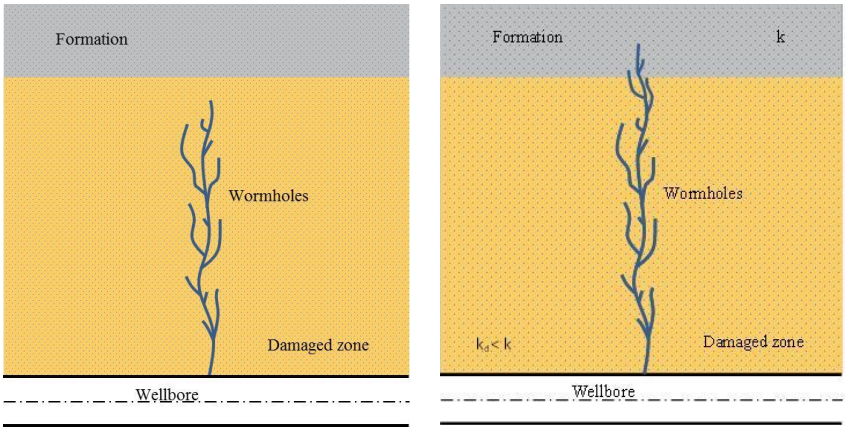

Fig. 27 Wormhole region inside the damaged zone (Tran, 2013)

The plot (d) in **Fig. 29** indicates wormhole created inside of damaged region during early time thus skin was still huge effect thus bottomhole pressure is still high but the values of both pressure and skin converges to lower values after wormhole penetrates longer than damaged region and not sensitive anymore.

(e) Damage penetration radius (r_d):

As same reason with (d), Eq. (2.45) shows deeper damage radius provides higher skin. After wormhole penetrate damage radius, bottomhole pressure and skin is converged.

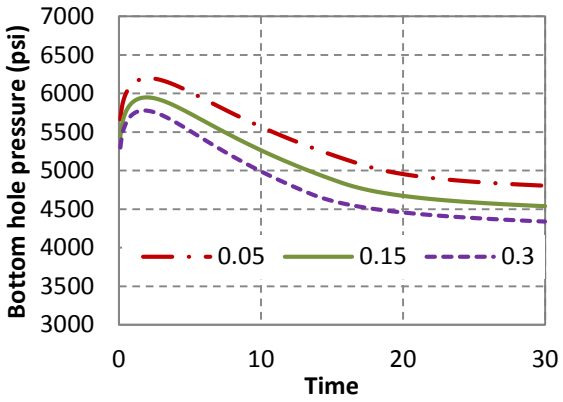

(a) Porosity

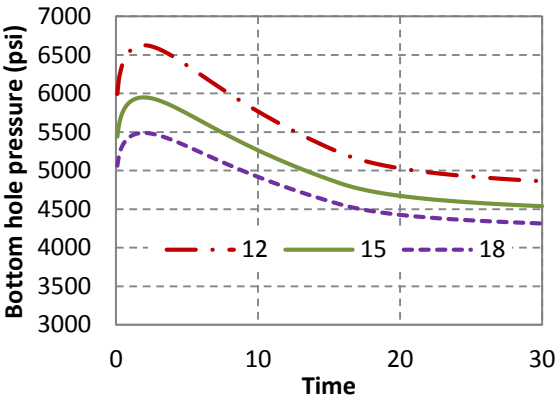

(b) Horizontal Permeability

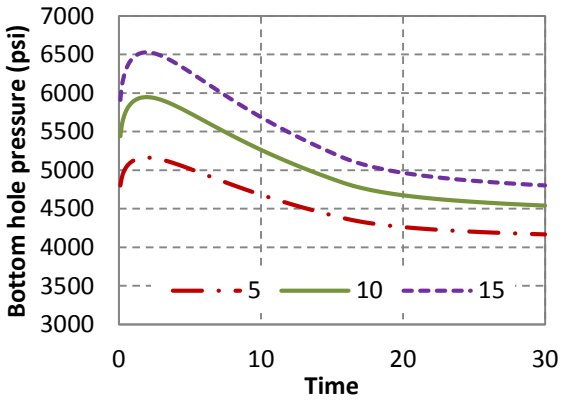

(c) Permeability Ratio (k_h/k_v)

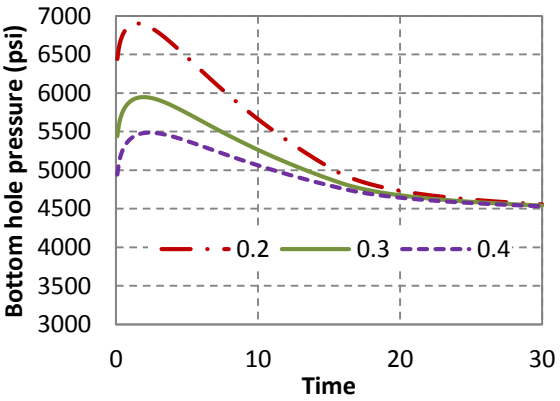

(d) Permeability Impairment Ratio (k_s/k)

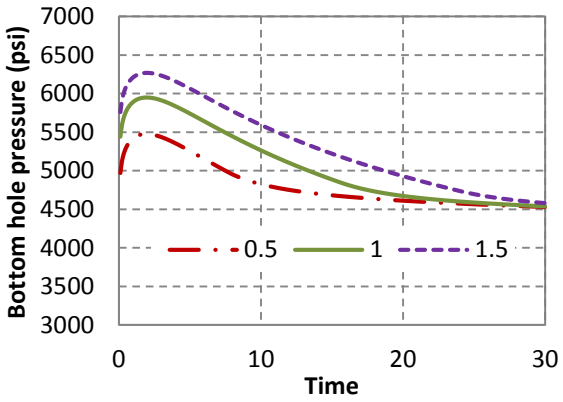

(e) Damage Penetration Radius

Fig. 28 Pressure-dependent sensitivity on reservoir and near-wellbore parameter

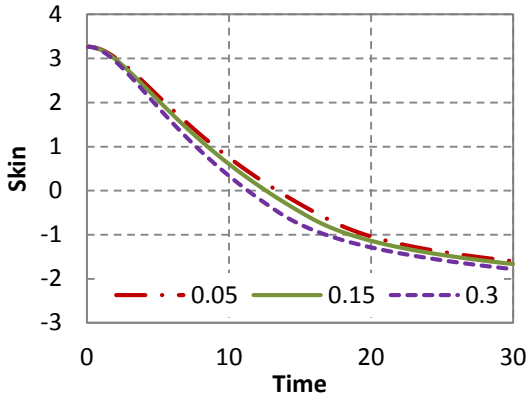

(a) Porosity

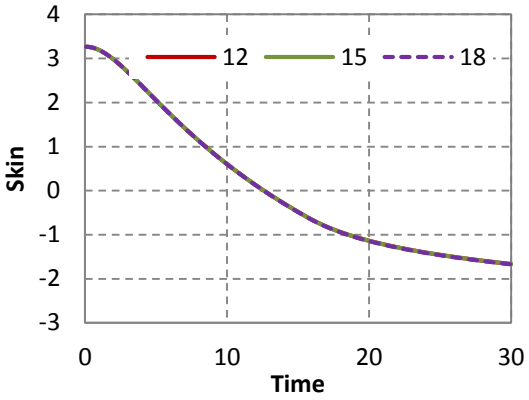

(b) Horizontal Permeability

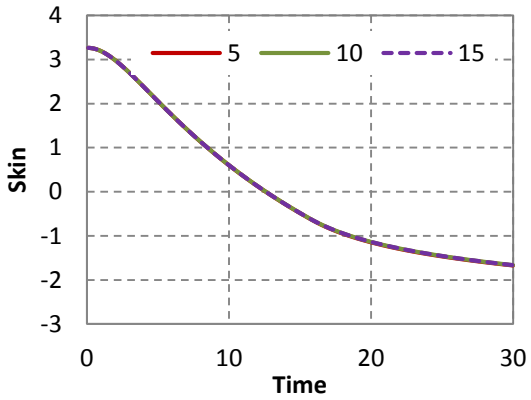

(c) Permeability Ratio (k_h/k_v)

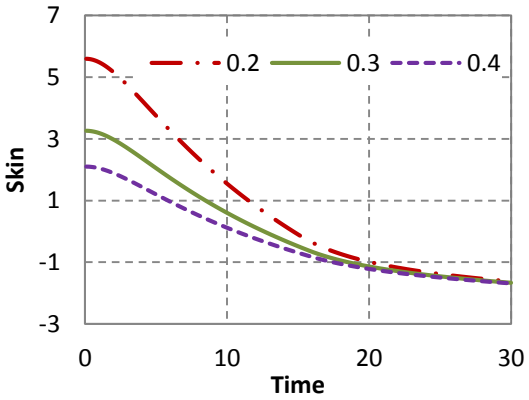

(d) Permeability Impairment Ratio (k_s/k)

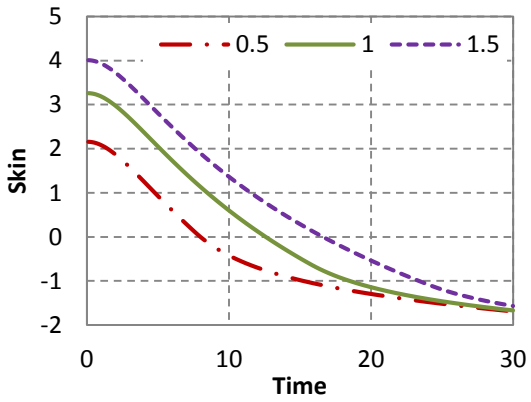

(e) Damage Penetration Radius

Fig. 29 Skin-dependent sensitivity of reservoir and near-wellbore parameter

2.4.1.2. Wormhole Model Parametric Sensitivity Study

The results of pressure and skin dependent sensitivity for Furui's wormhole model parameters are summarize in Fig. 30 and Fig. 31. It is observed that the overall behavior of skin-dependent sensitivity is same as pressure-dependent sensitivity. The description of each parameter effect on pressure and skin is as follows.

(a) Optimum pore volume to breakthrough ($PV_{bt\text{-}opt}$):

The relation of the average growth rate of the wormhole front, V_{wh} and PV_{bt} is given by:

$$PV_{bt} = \frac{V_i}{V_{wh}} \tag{2.46}$$

After each data point of PV_{bt} and V_i is obtained, the minimum point is obtained by fitting the wormhole model to the results of laboratory tests. This lowest point defines the optimum condition (optimal pore volume to breakthrough, $PV_{bt\text{-}opt}$, and optimal interstitial velocity, $V_{i\text{-}opt}$) . It should be noted that $PV_{bt\text{-}opt}$ is only an optimum in volume and smallest volume of acid required for wormhole breakthrough.

Considering Eq.(2.46) an (2.47), smaller $PV_{bt\text{-}opt}$ generates higher wormhole velocity at the tip thus skin drops faster and botomhole pressure deceases faster as well.

$$v_{i,tip,opt} = \frac{v_{i,opt}}{PV_{bt,opt} N_{AC}} \frac{r_{wh}}{L_{core}} \tag{2.47}$$

(b) Optimum interstitial velocity ($V_{i,opt}$):

Eq.(2.47) shows higher $V_{i\text{-}opt}$ generates higher $V_{i,tip,op.}$ According to the Eq.(2.46), V_{wh} is always an increasing function of V_i. Therefore, as Vi-opt is higher, wormhole propagate faster, reducing skin faster and botomhole pressure deceases faster as well.

(c) Wormhole axial-spacing coefficient (α_z):

In Furui wormhole model, the interstitial velocity at wormhole tip under radial flow condition is approximated as Eq. (2.48), which assumes that in-situ injection velocity at the tip of wormholes would be much higher than that predicted by conventional radial flow.

$$v_{i,tip} = \frac{q}{\phi L\sqrt{\pi m_{wh}}}\left[(1-\alpha_Z)\frac{1}{\sqrt{d_{e,wh}r_{wh}}} + \alpha_Z\left(\frac{1}{d_{e,wh}}\right)\right] \tag{2.48}$$

where, α_z is defined by the FEM simulation result as follows

$$\alpha_Z = \left(\frac{h_{wh}}{r_{wh}}\right)^{0.7} \tag{2.49}$$

α_z is set to be 0 for wormholes closely spaced in the axial direction, while α_z is set to be 1 for wormholes sparsely distributed in the axial direction. As α_z is larger, dominant wormhole structure is assumed and $V_{i,tip}$ should be faster compared with conventional radial flow. Therefore, wormhole propagation would be faster and pressure and skin decreased faster.

(d) Effective wormhole diameter ($d_{e,wh}$):

$d_{e,wh}$ is actual wormhole diameter inside of wormhole conduit as seen in **Fig. 30**. $d_{e,wh}$ has significant impact on $V_{i,tip}$ in radial geometry as seen in Eq.(2.48). Smaller diameter gives higher velocity. Therefore, as diameter becomes smaller and wormhole propagates faster, so that the pressure and skin decline faster.

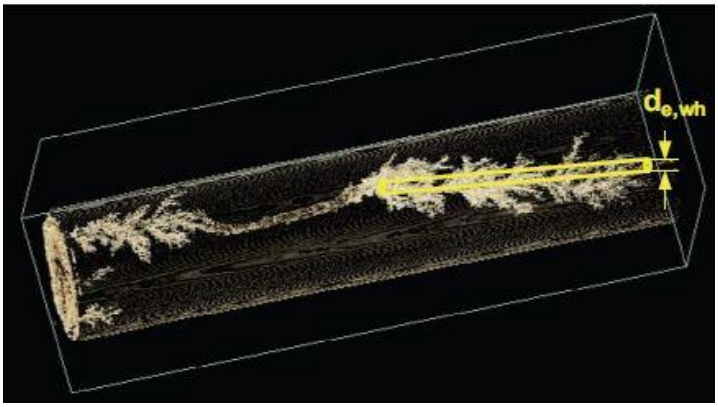

Fig. 30 CT scan of wormhole conduit on core-flooding (Furui et al. 2012)

(e) Number of dominant wormhole per 2D or 3D plane (m_{wh}):

Furui's model assumes m_{wh} is symmetry as shown in **Fig. 31**. It has been observed in the literature that a few dominant wormholes grow and are spaced apart in both angular and axial directions in a certain pattern under radial flow conditions. Eq. (2.48) implies that $V_{i,tip}$ decreases as m_{wh} increases because of injection-fluid competition mechanism.

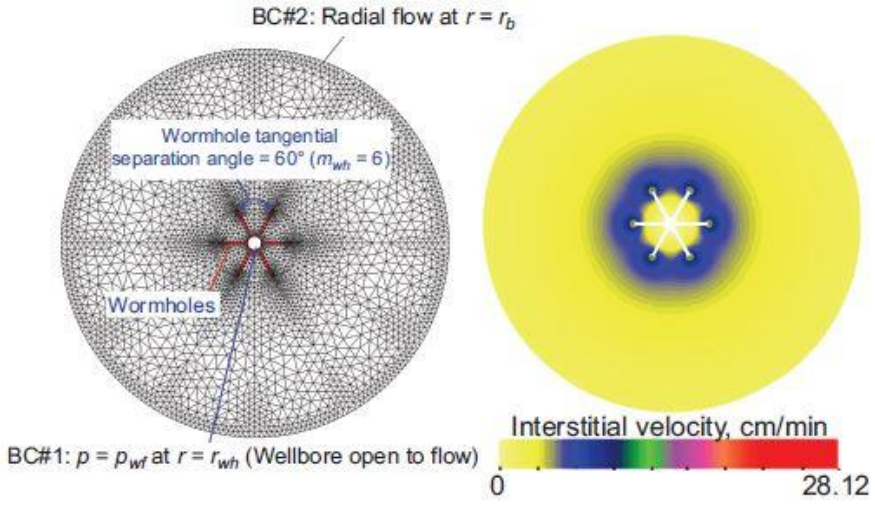

Fig. 31 Velocity contour plot on 2D radial flow with m_{wh} = 6. (Furui, 2012)

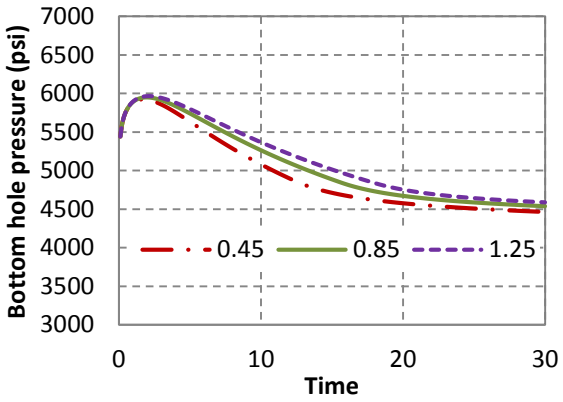

(a) Optimum pore volume to breakthrough

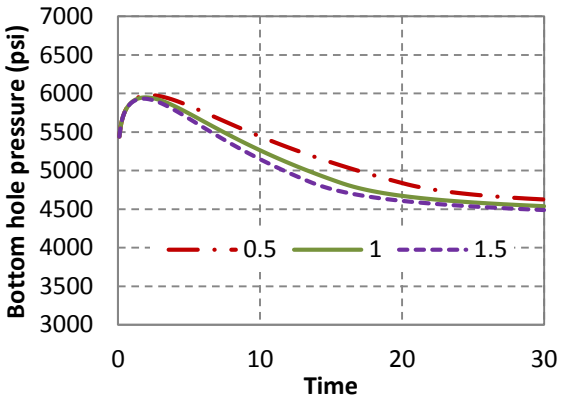

(b) Optimum interstitial velocity

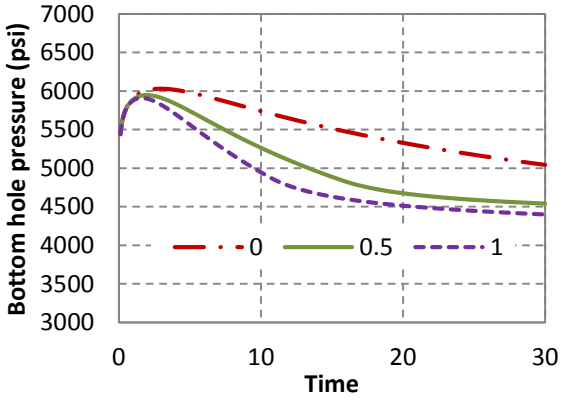

(c) Wormhole axial-spacing coefficient

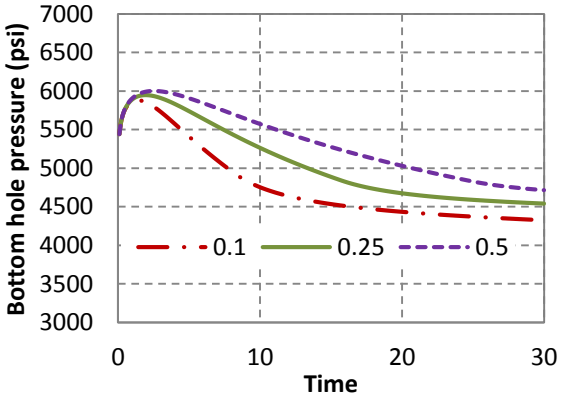

(d) Effective wormhole diameter

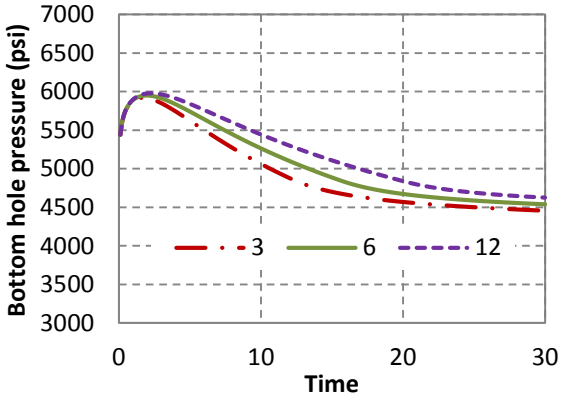

(e) No. of Dominant wormholes

Fig. 32 Pressure-dependent sensitivity on wormhole model parameter

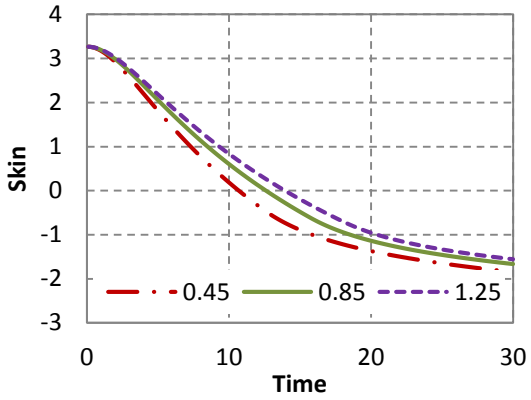

(a) Optimum pore volume to breakthrough

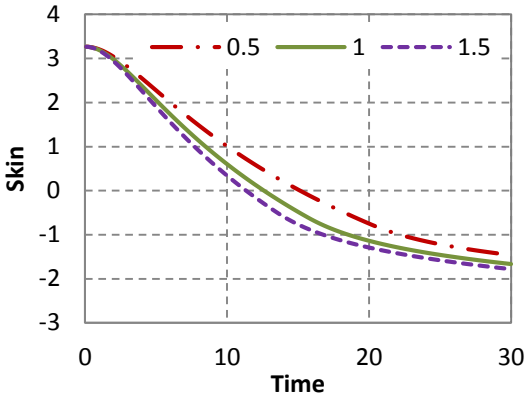

(b) Optimum interstitial velocity

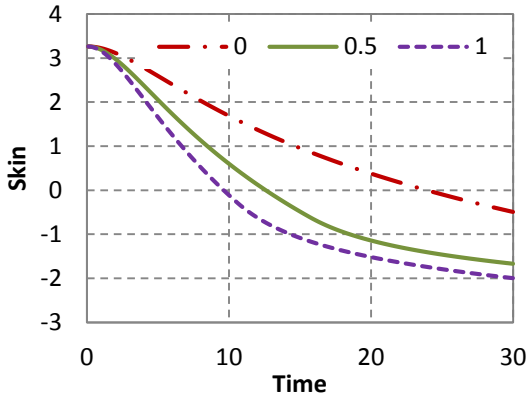

(c) Wormhole axial-spacing coefficient

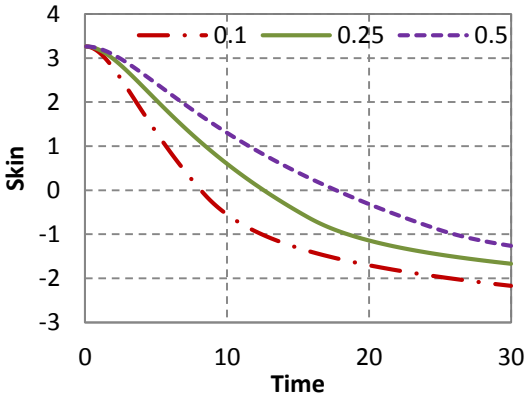

(d) Effective wormhole diameter

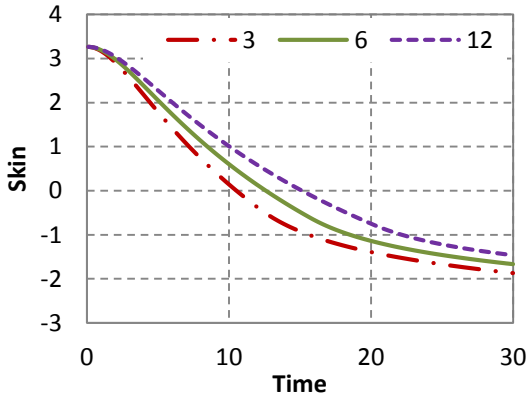

(e) No. of Dominant wormholes

Fig. 33 Skin-dependent sensitivity of wormholing model parameter

2.4.2. History Matching Process

The result of sensitivity analysis shows that in openhole condition, damage related parameters such as permeability impairment ratio (k_s/k) and damage radius (r_d) are sensitive during early time period until wormhole penetrates the damage region. Reservoir parameters such as porosity and permeability are sensitive during entire stimulation period. On the other hands, among wormholing parameters used in the Furui model, wormhole axial-spacing coefficient (α_z) and the effective wormhole diameter (d_{ewh}) are recognized as most uncertain parameters.

Table 7 shows how to measure each parameter before a stimulation. As recognized, α_z is inherently not given parameter in lab condition but should be obtained by history matching process under the radial flow condition in field scale. Number of Dominant Wormholes, m_{wh} cannot be measured in the linear core-flooding experiment, but it does not affect the result significantly so that it is assumed to use a suggested number.

Table 7 Measurement type of each parameter set

Parameter	Well Logging	Core flooding	Fall-off test
Porosity, ϕ	✓	✓	-
Horizontal Permeability, k_H (md)	✓	✓	✓
Permeability Impairment ratio, k_S/k	✓	-	-
Permeability Ratio, k_H/k_V	✓	-	-
Damage Penetration Radius, r_d (ft.)	✓	-	-
Optimum Pore Volume to Breakthrough, $PV_{bt\text{-}opt}$	-	✓	-
Optimum interstitial velocity, $V_{i\text{-}opt}$ (cm/min)	-	✓	-
Effective wormhole diameter, $d_{e,wh}$ (in.)	-	✓	-
No. of Dominant Wormholes, m_{wh}	-	Radial	-
Wormhole axial-spacing coefficient, α_z	-	-	-

2.4.3. Case Study

The limited entry case study shown in 2.2.4 is used as a history matching case study. As described before, wormhole axial-spacing coefficient (α_z) is the parameter that is optimized in the study. In this history matching, the same values of all parameters presented by Furui at el (2010) were used. Note that this case is limited entry and the well is hydraulically fractured before matrix acidizing, and it is assumed that damage parameters does not affect the pressure behavior. The input parameters are shown in **Table 8**.

Table 8 Wormholing parameter inputs

Inputs	Value
Optimum Pore Volume to Breakthrough, $PV_{bt\text{-}opt}$	0.393
Optimum interstitial velocity, $V_{i\text{-}opt}$ (cm/min)	1.468
Effective wormhole diameter, $d_{e,wh}$ (in.)	0.1
No. of Dominant Wormholes, m_{wh}	6

For this case study, integrated limited entry function introduced in 2.2.3 was used. The result of pressure history matching is shown in **Fig. 34**. This match was obtained with α_z set to 0.75. The correspondent result of skin history match is in **Fig. 35**. Due to the friction reducer effect, actual reservoir face pressure is fluctuated but the entire match trend is acceptable.

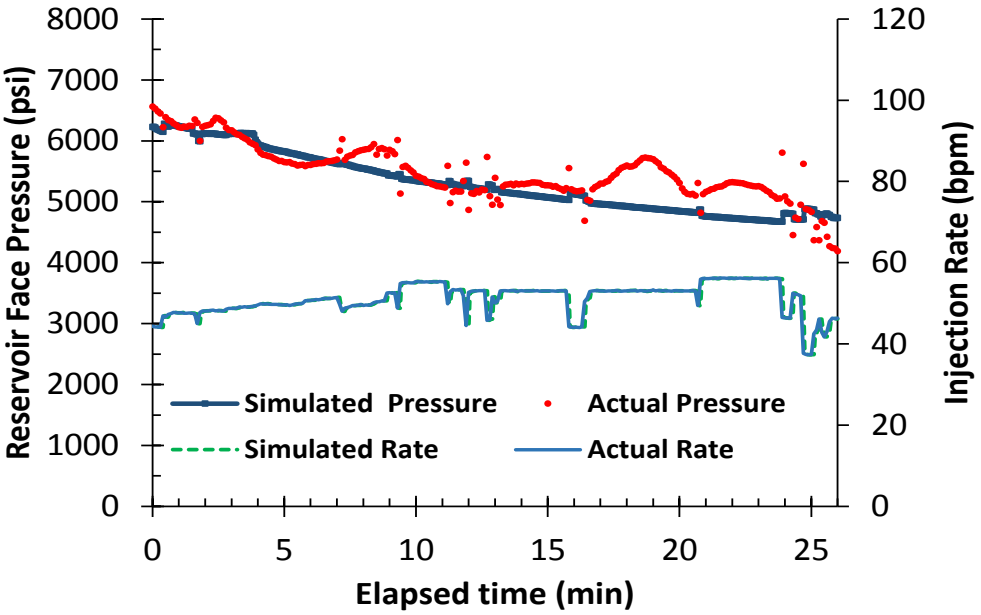

Fig. 34 Pressure match result

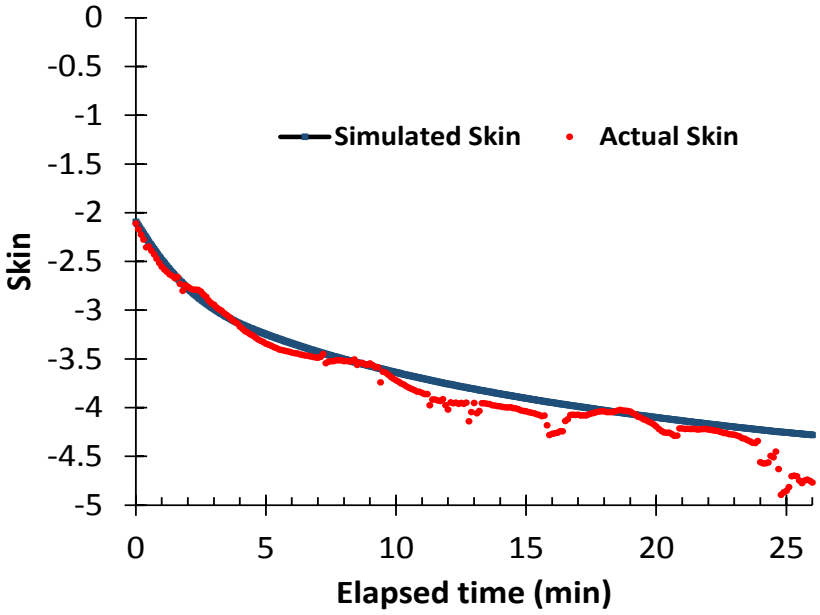

Fig. 35 Skin match result

2.5. Integrated Optimization

After finishing the history match process, wormhole axial-spacing coefficient fitted by the actual field condition is obtained. Tran (2013) studied the optimum wormhole propagation conditions of matrix acidizing treatments in carbonate formations and compared acid distribution and wormhole penetration along the wellbore for the increasing rate injection to those of a constant optimum rate (determined in the parametric study), and to a constant maximum allowable rate below the fracture gradient of the formation. He showed that the rate needs to be increasing as more acid is injected into the formation. It actually followed the study of Furui (2010) that showed the wormhole growth rate decreases as the acid spends in the formation, yielding lower efficient wormhole propagation over time. If we inject acid at a constant (even the optimum) injection rate, the interstitial velocity at the tip of wormholes decreases as injection time increases. To keep the wormhole growth process at the optimum conditions, the interstitial velocity needs to be maintained at or close to its optimum as the wormhole length increases.

2.5.1. Optimum Rate Calculation

For Furui's model, the growth rate of a wormhole extending around the wellbore is given as,

$$v_{wh} = v_{i,tip} N_{AC} \left(\frac{v_{i,tip} PV_{bt,opt} N_{AC}}{v_{i,opt}} \right)^{-\gamma} \times \left\{ 1 - \exp\left[-4 \left(\frac{v_{i,tip} PV_{bt,opt} N_{AC} L_{core}}{v_{i,opt} r_{wh}} \right)^2 \right] \right\}^2 \qquad (2.50)$$

Assuming the diffusion limited reaction is the dominant process, the optimum tip velocity is,

$$v_{i,tip,opt} = \frac{v_{i,opt}}{PV_{bt,opt} N_{AC}} \frac{r_{wh}}{L_{core}} \tag{2.51}$$

The goal of the optimum acidizing treatment design is to maintain the wormhole propagation at its optimum conditions. Especially for Furui's model, wormhole tip is satisfied with optimum condition all the time. Thus,

$$v_{i,tip} = v_{i,itp-opt} \tag{2.52}$$

Replacing Eq. (2.50) with Eq. (2.52) and (2.53) when the fluid loss limited wormholing, $\gamma = 1/3$,

$$v_{wh} = v_{i,tip,opt} N_{AC} \left(\frac{v_{i,tip,opt} PV_{bt,opt} N_{AC}}{v_{i,opt}} \right)^{-\frac{1}{3}} \times \left\{ 1 - \exp\left[-4 \left(\frac{v_{i,tip,opt} PV_{bt,opt} N_{AC} L_{core}}{v_{i,opt} r_{wh}} \right)^2 \right] \right\}^2 \tag{2.53}$$

Then substituting Eq. (2.51) in to Eq. (2.53),

$$v_{wh} = \frac{v_{i,opt}}{PV_{bt,opt}} \left(\frac{r_{wh}}{L_{core}} \right)^{\frac{2}{3}} \times \left[1 - \exp(-4) \right]^2 \tag{2.54}$$

When second term of Eq. (2.54) is simplified,

$$v_{wh} = 0.96 \left(\frac{v_{i,opt}}{PV_{bt,opt}} \right) \left(\frac{r_{wh}}{L_{core}} \right)^{\frac{2}{3}} \tag{2.55}$$

From the Eq. (2.55), it is noticed that the wormhole growth rate depends on the wormhole penetration radius and the length of the core. Assuming in a time increment Δt during which the wormhole growth rate V_{wh} is constant, the wormhole penetration can be calculated by,

$$r_{wh}^{n+1} = r_{wh}^{n} + v_{wh} \Delta t \tag{2.56}$$

From the wormhole penetration we can calculate the optimal injection rate as a function of time. Finally, a theoretical incremental rate schedule in radial flow regime is calculated by,

$$q^{n+1} = \frac{v_{i,tip,opt}\phi L\sqrt{\pi m_{wh}}}{\left[(1-\alpha_Z)\frac{1}{\sqrt{d_{e,wh}r_{wh}}} + \alpha_Z\left(\frac{1}{d_{e,wh}}\right)\right]} \tag{2.57}$$

Practically speaking, it was noted in the literature (Glasbergen et al.,2009) that the reservoir pressure should be fairly uniform, the total zone height should be relatively short, and no major variations in permeability should be present in order to be a candidate for applying the optimum injection rate. Otherwise, maximum rate should be used.

2.5.2. Case Study

Using same the limited entry case as treatment monitoring and history matching, the optimum rate schedule is formulated based on the derivation in section 2.5.1. In this case study, the effectiveness of calculated increasing rate schedule has been compared with the case of both the maximum injection rate available in operated condition and the actual treated injection rate. For the comparison, three injection rate schedule are shown in **Fig. 36**. It is noted that increasing rate is going to be flat because of the constraint of maximum rate possible after 9 minutes. For the increasing rate schedule, the optimum rate is increasing in a fast pace if one want to keep the optimum wormhole tip condition.

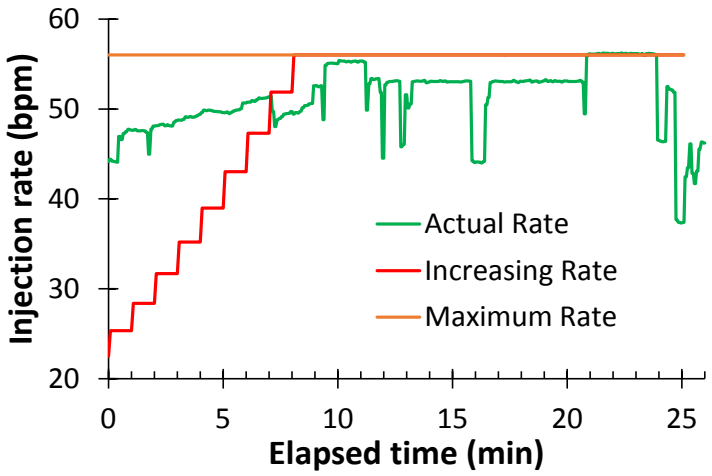

Fig. 36 Rate schedule comparison

Fig. 37 shows the comparison of skin evolution based on the rate schedule. It is observed that final skin evolutions are converged in 26 minutes because all the rate reached the maximum rate. This means that the total acid volume used in increasing rate schedule may be the least volume among the three rate patterns.

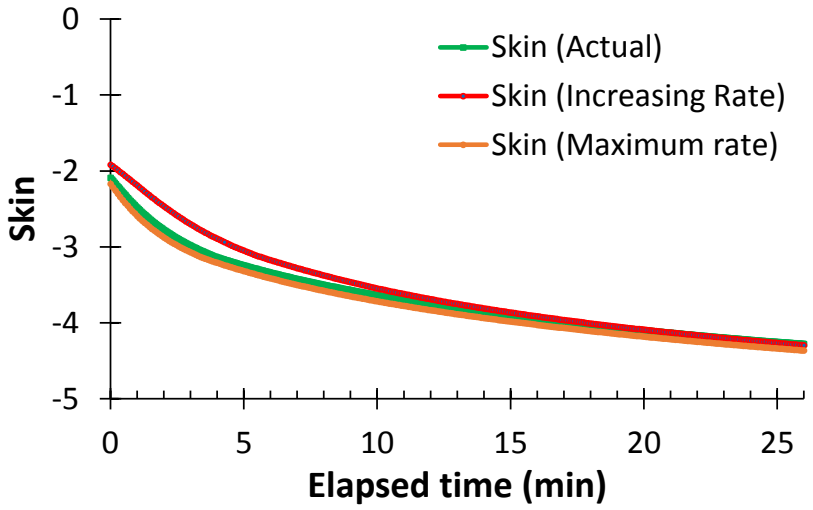

Fig. 37 Skin evolution comparison

However, it should be noted that the increasing rate schedule was estimated based on the assumption that flow pattern is always radial flow and reservoir pressure is fairly uniform, the total zone height is relatively short, and no major variations in the permeability.

There may exist deviations in the reality from these assumptions. Since this case was limited entry and short fractures were created before matrix acidizing, higher rate to satisfy optimum spherical flow may be necessary.

3. EVALUATION OF ACID FRACTURING THROUGH TREATMENT MONITORING AND PRODUCTION ANALYSIS

3.1. Introduction

Unlocking tight carbonate formations for oil and gas production by multi-stage acid fracturing in horizontal wells is relatively cost-effective as alternative to the use of proppants. Real-time assessment of skin evolution in carbonate reservoir during matrix acidizing treatment has been successfully applied in the industry in vertical and horizontal wells however an extended applicability of skin evolution analysis from matrix acidizing to acid fracturing (above closure pressure) is limited. Since fracturing can be approximated move to a linear flow patter rather than radial flow for matrix acidizing, another method should be developed to monitor in real-time.

In this chapter, new method for real-time monitoring of acid fracturing, the inverse injectivity vs. superposition time function plot is presented, subject to the condition that the treatment pressure is above closure pressure after the breakdown. A linear dual-porosity transient slab model to simulate rate transient response in hydraulically fractured horizontal wells normally used in production analysis has been applied for horizontal well stimulation performance that can be implemented for field evaluation of acid fracturing treatment. Using that model with injectivity methodology, actual growing "cross-sectional area" by acid fracturing treatment can be monitored in real-time. The treatment is subject to be transient flow occurred in early time thus cross-sectional area from injection flow

has been identified as real-time monitoring parameter, assuming bilinear flow regime occurred during injection.

By monitoring cross-sectional area from injection flow, its real-time area growth induced by acid fracturing is monitored during acid fracturing treatment. Even if the condition such that pressure fluctuates around closure pressure, which makes it difficult to identify whether fracture is closed or open, monitoring both existent skin evolution under matrix acidizing and acid fracturing effect allows us to observe the effect of acid stimulation comprehensively. Another benefit of selecting cross-sectional area as a monitoring parameter is that one can examine the stimulation effectiveness by conducting production data analysis after production starts. Linear flow diagnostic approach with Rate-Transient Analysis provides cross-sectional area flowing from matrix, which is compared with the area induced by acid fracturing in real-time. The treatment efficiency provides engineers with additional information as to whether the designed acid fracturing was performed appropriately under the in-situ closure stress field.

3.2. Treatment Monitoring in Acid Fracturing in Horizontal Well

3.2.1. Dual-Porosity Transient Slab Model

The purpose of this section is to introduce analyzing a fracturing treatment in horizontal well with same monitoring method approach shown in matrix acidizing. Using the transient dual porosity solution which is most commonly used in the literature in rate transient analysis for a linear model originally presented by El-Banbi and extended by

Bello and Wattenbarger as shown in **Fig. 38**, necessary flow regime occurring during fracturing treatment was incorporated to existing method.

However skin over time during acid fracturing treatment is difficult to be generated conceptually because fracturing skin is given by pseudo radial flow. Our treatment is subject to be transient flow occurred in early time thus cross-sectional area from injection flow has been identified as real-time monitoring parameter. Monitoring cross-sectional area from injection flow, its real-time growth is monitored during acid fracturing treatment. If we assume rectangular shape of fracture, approximate fracture half-length is monitored in real-time. Using a field example, we demonstrate the augmented method be consistent and useful.

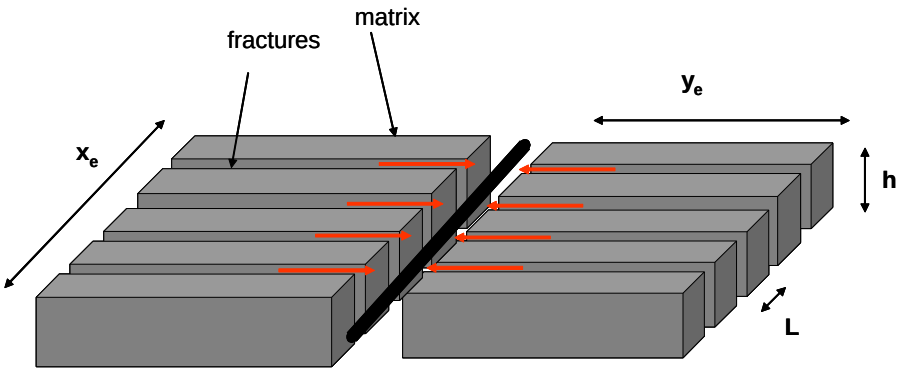

Fig. 38 Schematic of slab matrix linear model well (Bello, 2009)

The transient dual porosity solutions presented here for a linear model was seen in the literature (El-Banbi, 1998). Bello and Wattenbarger extended the model towards an actual multi-fractured horizontal well, which has the advantage of being simpler than other horizontal well models and allows relaxing five flow-regime. The diffusivity equations

for the matrix and fracture are solved in Laplace space. Although mathematical details of the linear dual porosity model (slab matrix) are found in the literature (Bello, 2009), the constant rate inner boundary and closed outer boundary reservoir (slab matrix) solution in Laplace space is given in Eq. (3.1).

$$\overline{p_{wDL}} = \frac{2\pi}{u\sqrt{uf(u)}}\left[\frac{1+e^{-2\sqrt{uf(u)}y_{De}}}{1-e^{-2\sqrt{uf(u)}y_{De}}}\right] \tag{3.1}$$

where, dual porosity parameters for the slab matrix case,

$$f(u) = \omega + \sqrt{\frac{\lambda_{Ac}}{3u}(1-\omega)}\tanh\sqrt{\frac{3(1-\omega)u}{\lambda_{Ac}}} \tag{3.2}$$

$$\lambda_{Ac} = \frac{12}{L^2}\frac{k_m}{k_f}A_c \tag{3.3}$$

$$\omega = \frac{(\phi\ c_t)_f}{(\phi\ c_t)_f + (\phi\ c_t)_m} \tag{3.4}$$

It is defined that *f(u)* is a Laplace space function used in transient dual porosity model. λ_{AC} is the Warren and Root dimensionless interporosity flow parameter and controls how fast the fluid drains from the matrix to the fractures and ω is dimensionless storativity ratio and controls how much fluid is initially in the fracture system. In our analytical model, flow-regime assumes to be bilinear flow which has simultaneous transient flow in the fracture system and matrix.

The following dimensionless variables for gas reservoir are defined to convert dimensionless pressure and time into pressure and time in real space. Note that A_c is defined as cross-sectional area to flow. It is noted that unit of t is hours when 0.000264.

$$t_{DAc} = \frac{0.000264 k_f t}{(\phi \mu c_t)_{f+m} A_c} \tag{3.5}$$

$$m_{DL} = \frac{k_f \sqrt{A_c}\,[m(p_i) - m(p_{wf})]}{1422 q_g T} \tag{3.6}$$

$$y_{De} = \frac{y_e}{\sqrt{A_c}} \tag{3.7}$$

Since injection pressure is normally more than 3,000 psi, the pseudo pressure in Eq. (3.6) can be converted into single pressure as follows:

$$p_{DL} = \frac{k_f \sqrt{A_c}\,(p_i - p_{wf})}{1422 q_g T}\left(\frac{2 p_i}{\mu_i z_i}\right) \tag{3.8}$$

3.2.2. Bilinear Analytical Model

In a fracturing treatment with injected liquid, bilinear flow caused by simultaneous transient flow into the fracture system and matrix is assumed.

The derivation of constant rate solution for bilinear flow regime are shown as below. Starting with Eq. (3.1) again,

$$\overline{p_{wDL}} = \frac{2\pi}{u\sqrt{uf(u)}}\left[\frac{1 + e^{-2\sqrt{uf(u)}\,y_{De}}}{1 - e^{-2\sqrt{uf(u)}\,y_{De}}}\right] \tag{3.9}$$

This can be shown to be the same as:

$$\overline{p_{wDL}} = \frac{2\pi}{u\sqrt{uf(u)}}\,Coth\left(\sqrt{uf(u)}\,y_{De}\right) \tag{3.10}$$

where,

$$Coth(x) = \frac{e^{2x} + 1}{e^{2x} - 1} \tag{3.11}$$

With approximately for x>3, $Coth\ (x) \approx 1$. Eq. (3.10) becomes,

$$\overline{p_{wDL}} = \frac{2\pi}{u\sqrt{uf(u)}} \tag{3.12}$$

For slab matrix:

$$f(u) = \omega + \sqrt{\frac{\lambda_{Ac}}{3u}(1-\omega)}\tanh\sqrt{\frac{3(1-\omega)u}{\lambda_{Ac}}} \tag{3.13}$$

Assuming $\omega << \sqrt{\frac{\lambda_{Ac}}{3u}(1-\omega)}\tanh\sqrt{\frac{3(1-\omega)u}{\lambda_{Ac}}}$ then, $1-\omega \approx 1$

Approximately for x >3, $\tanh\ (x) \approx 1$. Since $\frac{3(1-\omega)u}{\lambda_{Ac}} > 3$, $\tanh\sqrt{\frac{3(1-\omega)u}{\lambda_{Ac}}} \approx 1$.

Therefore substituting those assumptions into Eq. (3.13), the simplified form is,

$$f(u) = \sqrt{\frac{\lambda_{Ac}}{3u}} \tag{3.14}$$

Then substituting Eq. (3.14) into Eq. (3.12):

$$\overline{p_{wDL}} = \frac{2\pi}{uu^{0.5}\left(\frac{\lambda_{Ac}}{3u}\right)^{0.25}} = \frac{(2\pi)(3)^{0.25}}{u^{1.25}\lambda_{Ac}{}^{0.25}} \tag{3.15}$$

Mathematically,

$$\ell^{-1}\left\{\frac{1}{u^{1.25}}\right\} = \frac{t^{1.25-1}}{\Gamma(1.25)} = \frac{t^{0.25}}{0.9064} \tag{3.16}$$

$$\ell^{-1}\left\{\frac{1}{u}\right\} = 1 \tag{3.17}$$

Inverting from Laplace to real space:

$$p_{wDL} = \frac{(2\pi)(3)^{0.25}}{0.9064\lambda_{Ac}{}^{0.25}}t_{DAc}^{0.25} = \frac{9.12305}{\lambda_{Ac}{}^{0.25}}t_{DAc}^{0.25} \tag{3.18}$$

Eq. (3.18) is dimensionless constant rate solution for bilinear flow model.

3.2.3. Approach

Derived Eq. (3.18) is applied to the treatment monitoring methodology by Zhu and Hill (1996, 1998). One big difference with production analysis, however, is that fracture keeps growing, thus the area of fracture, A_c is not a constant as depicted in **Fig. 39**.

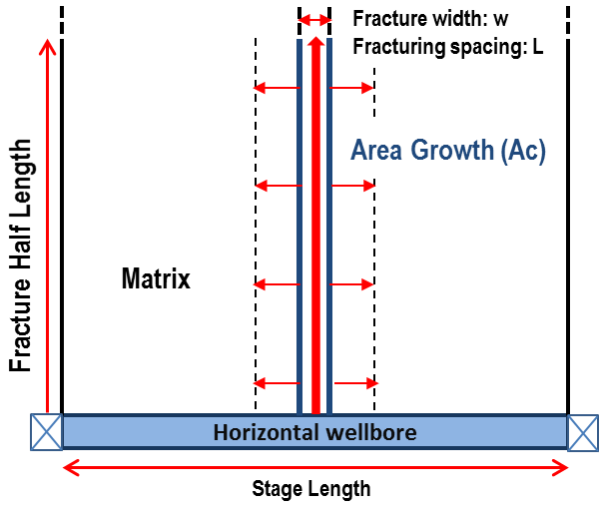

Fig. 39 Stimulation schematic (Plan view)

Using Eq. (3.5) and (3.8), Eq. (3.18) is re-written in linear relationship, noting that quadratic root of time is used as superposition time function because of bilinear flow. Applying the dimensionless pressure definition to convert to real pressure:

$$\frac{k_f\sqrt{A_c}\left(p_{wf}-p_i\right)}{1422q\,T}\left(\frac{2p_i}{\mu_i z_i}\right)=\frac{9.12305}{\lambda_{Ac}^{\,0.25}}t_{DAc}^{0.25} \tag{3.19}$$

where, k_f is adopted as effective fracture permeability (Kazemi, 1969) in fracture spacing, L.

$$k_f = \frac{w k_f + (l-w) k_m}{L} \approx \frac{w k_f}{L} \tag{3.20}$$

Since in the direction perpendicular to the transverse fracture, the flow from high conductive fracture region is restricted to low matrix permeability region, weighted average permeability is reasonable in the dual porosity model.

Rearranging Eq. (3.19),

$$\frac{p_{wf} - p_i}{q} = \frac{1422T}{k_f \sqrt{A_{cw}}} \left(\frac{\mu_i z_i}{2 p_i} \right) \frac{9.12305}{\lambda_{Ac}^{0.25}} t_{DAc}^{0.25} \tag{3.21}$$

Substituting dimensionless time of Eq. (3.5) into Eq. (3.21):

$$\frac{p_{wf} - p_i}{q} = \frac{1422T}{k_f \sqrt{A_c}} \left(\frac{\mu_i z_i}{2 p_i} \right) \frac{9.12305}{\lambda_{Ac}^{0.25}} \left[\frac{0.000264 k_f}{(\phi \mu c_t)_{f+m} A_c} \right]^{0.25} t^{0.25} \tag{3.22}$$

where,

$$\lambda_{Ac} = \frac{12}{L^2} \frac{k_m}{k_f} A_c \tag{3.23}$$

Rearranging the Eq. (3.22) for A_c,

$$\frac{p_{wf} - p_i}{q} = \frac{1}{A_c^{0.75}} \frac{1422T}{k_f} \left(\frac{\mu_i z_i}{2 p_i} \right) \frac{9.12305}{\left(\frac{12}{L^2} \frac{k_m}{k_f} A_c \right)^{0.25}} \left[\frac{0.000264 k_f}{(\phi \mu c_t)_{f+m}} \right]^{0.25} t^{0.25} \tag{3.24}$$

$$\frac{p_{wf} - p_i}{q} = \frac{1}{A_c} \frac{1422T}{\sqrt{k_f}} \left(\frac{\mu_i z_i}{2 p_i} \right) \frac{9.12305\sqrt{L}}{(12 k_m)^{0.25}} \left[\frac{0.000264}{(\phi \mu c_t)_{f+m}} \right]^{0.25} t^{0.25} \tag{3.25}$$

Now superposition time function is written as usual,

$$\Delta t_{\text{sup}} = \sum_{j=1}^{N} \frac{q_j - q_{j-1}}{q_N} \left(t_N - t_{j-1}\right)^{0.25} \tag{3.26}$$

Slope m is defined by Eq. (3.26).

$$m = \frac{1422T}{\sqrt{k_f}} \left(\frac{\mu_i z_i}{2p_i}\right) \frac{9.12305\sqrt{L}}{\left(12k_m\right)^{0.25}} \left[\frac{0.000264}{(\phi \mu c_t)_{f+m}}\right]^{0.25} \tag{3.27}$$

Rearranging again using superposition time, the following equation is obtained:

$$\frac{p_{wf} - p_i}{q} = \frac{1}{A_c} m\Delta t_{\text{sup}} \tag{3.28}$$

Finally cross sectional area to flow is obtained with reforming Eq. (3.28),

$$A_c(t) = \frac{m\Delta t_{\text{sup}}}{\frac{p_{wf} - p_i}{q}} \tag{3.29}$$

Assuming rectangular shape of fracture, cross sectional area to flow in bilinear flow regime is given as follows:

$$A_c(t) = 4wh + 4hx_f n_f \tag{3.30}$$

Since area of injection flow inside of fracture is much narrower than fracture-half length, first term of Eq. (3.30) should be minimized. Thus, A_c is approximated into:

$$A_c = 4wh + 4hx_f n_f \cong 4hx_f n_f \tag{3.31}$$

Thus, fracture half-length is obtained in each time step as:

$$x_f \cong \frac{A_c(t)}{4hn_f} \tag{3.32}$$

Summarizing the procedure to calculate real-time evolution of cross-sectional area from injection flow as a function of injection time by continuous monitoring of injection rates and pressures;

1. Calculate slope, m, using Eq. (3.27) for fractured horizontal wells in gas reservoir. The slope, m, is constant and depends on the reservoir parameters and dimension such as formation volume factor, permeability, and viscosity of the reservoir fluid.
2. From the measured pressure and injection rate at a desired time interval, calculate superposition time using Eq. (3.26) for horizontal wells.
3. Calculate cross-sectional area from injection flow using Eq. (3.29) at each time step.

3.2.4. Bilinear Flow Validation by Numerical Simulation

In this section, the assumed bilinear environment during injection treatment in hydraulically fractured reservoir is validated by the commercial numerical simulator. **Fig. 40** shows a finite-difference grid system employed in this work, where three transverse fractures with fracture half-length 250 ft. are set up but only toe stage is opened and simulated for the injection.

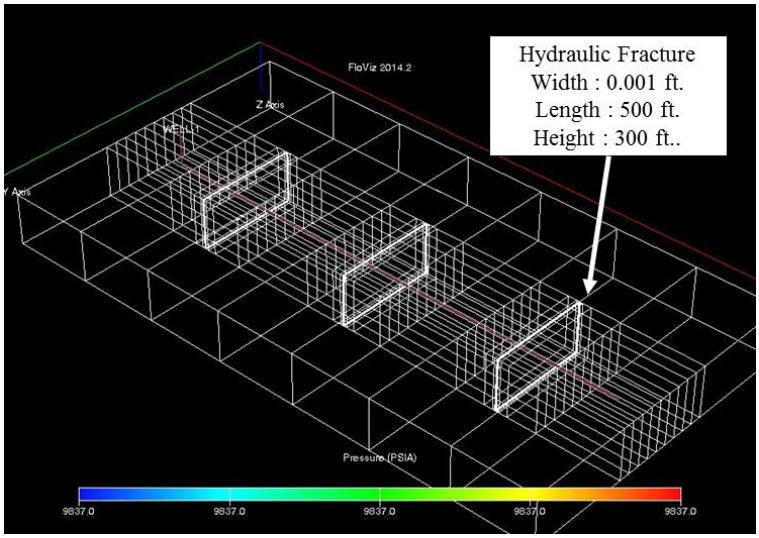

Fig. 40 Logarithmically spaced LGR grid system

To capture transient behavior occurred during injection, near-induced fracture region by acid fracturing is expressed by the logarithmically spaced local grid refinement (LGR). In this LGR model, the global grid which contains hydraulic fractures is divided into 21 different widths according to a logarithmically distribution in x direction. The table of input summary used in this work is shown below.

Table 9 Geometry of the simulation grid data

Parameters	Input Values
Dimensions	(nx,ny,nz) = (7,3,1)
Grid block size	(dx,dy,dz) = (400, 500, 300) ft
Matrix permeability	kx,ky,kz = 0.0044 md
Fracture permeability	kx,ky,kz = 2000 darcy
Fracture width	0.001 ft.

Table 10 Reservoir & simulation data

Reservoir Properties		Well and Stimulation Data	
Parameters	**Input Values**	**Parameters**	**Input Values**
Initial Reservoir Pressure	9837 psi	Wellbore Radius	3.307 in.
Formation Thickness	300 ft	Tubing Diameter	2.992 in.
Total Porosity	0.03	Stimulation Interval	400 ft
Total Compressibility	5.78E-05 1/psi	Reservoir top	20,000 ft
Initial Sw (matrix)	0.1	Injection fluid viscosity	1 cp
Initial Sw (Fracture)	1	Injection rate	15 bpm

Based on Brooks and Corey model, two relative permeability curves are set up for matrix and fracture respectively as shown in **Fig. 41**.

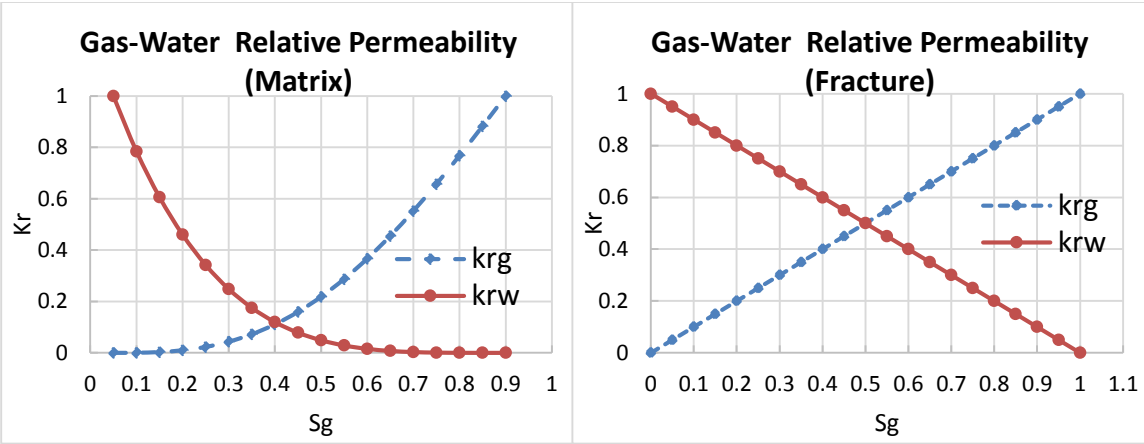

Fig. 41 Relative permeability for matrix and fracture

Fig. 42 is the plan view of pressure profiles around the wellbore from early time. It is seen that after the injected flow reached fracture-half length (250 ft.), fluid was expanded to x axis. Thus the assumption made in analytical model is validated.

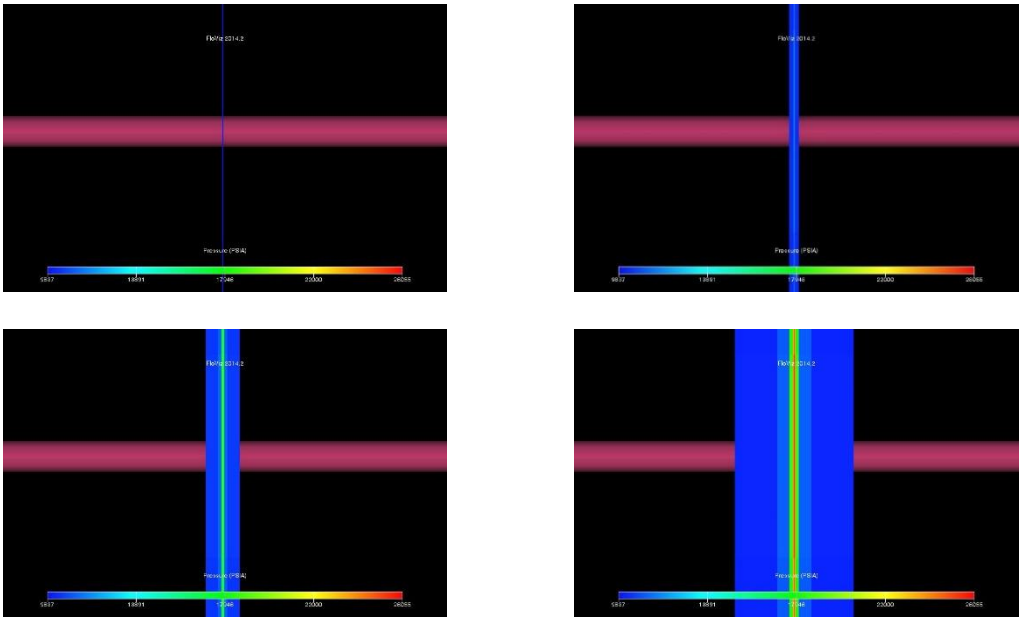

Fig. 42 Plan view of pressure shows bilinear flow

As the simulation result, **Fig. 43** shows that normalized rate vs. time plot in log-log scale. The diagnostic plot identifies ¼ slope which means that the flow regime during injection was bilinear. Thus, linear flow inside of the fracture and linear flow from the fracture to matrix occurs simultaneously. The deviation of early time is considered as infinite acting radial flow from the center of wellbore. After reaching the boundary, the flow was converged to bilinear flow.

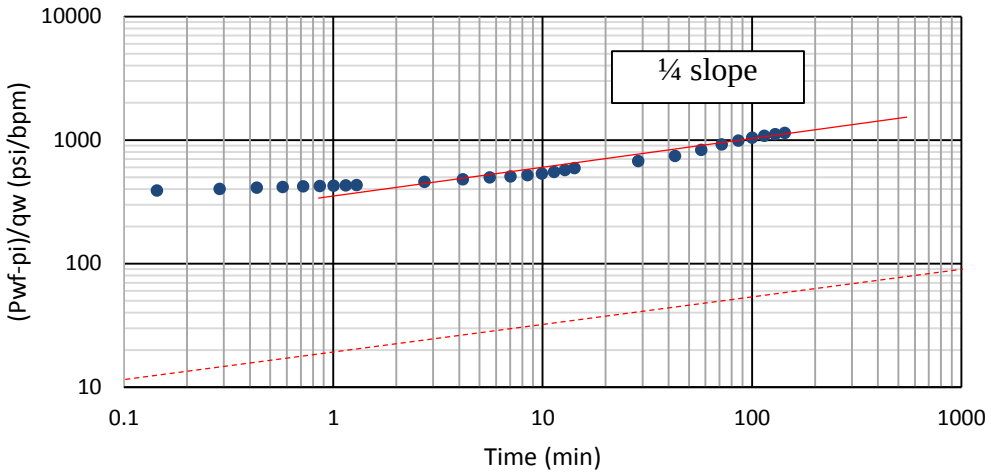

Fig. 43 Normalized rate plot during the injection

3.2.5. Case Study

3.2.5.1. Treatment Description

The acid stimulation in toe stage is analyzed and monitored. The input data for the reservoir, the wellbore for the analysis is summarized in **Table 11**.

Table 11 Input data for fracture monitoring

Reservoir Properties	
Parameters	**Input Values**
Initial Reservoir Pressure	9837 psi
Formation Volume Factor	0.003 ft3/scf
Total Porosity	0.03
Total Compressibility	5.78E-05 1/psi
Formation Thickness	250 ft.
Reservoir Fluid Viscosity	0.0315 cp
Reservoir Temperature	280 F
Z factor	1.36
matrix permeability	0.0044 md
fracture permeability (*)	2000 D
fracture width	0.001 ft.

Well and Stimulation Data	
Parameters	**Input Values**
Wellbore Radius	3.307 in.
Tubing Diameter	2.992 in.
Stimulation Interval	1,357 ft.
Vertical Depth	19,880 ft.
Measured Depth	23,343 ft.

(*) Effective permeability:

$$k_f = \frac{wk_f}{L} = \frac{2000[\text{md}\cdot\text{ft}]}{1357[\text{ft}]} = 1.5[\text{md}]$$

3.2.5.2. Monitoring Result

Fluid injection schedule from surface to measured depth at stage 1 is in **Table 12**.

Table 12 Treatment schedule of stage 1

Injection Schedule			
Stage	**Name**	**Viscosity, cp**	**Volume (gal)**
1	Gelled Acid	39	18492
2	X-linked acid	30	31701
3	Non-X-linked frac fluid	56	52834
4	X-linked acid	30	36984
5	Non-X-linked frac fluid	56	52834
6	Gelled acid	39	18492
7	Water Flush	1	5283

The surface tubing pressure and injection rate were measured on-site during the injection. Based on hydrostatic and friction pressure calculation by frictional pressure drop analysis made beforehand, the bottomhole pressure was generated in **Fig. 44**. As seen, each circle number corresponds to the fluid number in **Table 12** and each dashed line also corresponds to each fluid arrival at bottomhole.

It is noted that calculated reservoir face pressure fluctuates between the formation breakdown pressure and the closure pressure during the stimulation. It is also noted that the reservoir face pressure often decreased below the closure pressure but stayed around the closure pressure. The decision as to whether acid fracturing or matrix acidizing was happening strongly the calculated bottomhole pressure, breakdown, closure pressure and acid etched conductivity. Thus both matrix acidizing skin and cross-sectional growth induced by acid fracturing treatment were calculated in the monitoring process. Based on **Fig. 44** data, rate normalized plot in log-log scale is plotted to diagnose related flow regime. **Fig. 45** shows that after formation breakdown, bilinear flow occurred during acid injection. Fracture linear flow is identified when frac fluid used, which means fracture extension.

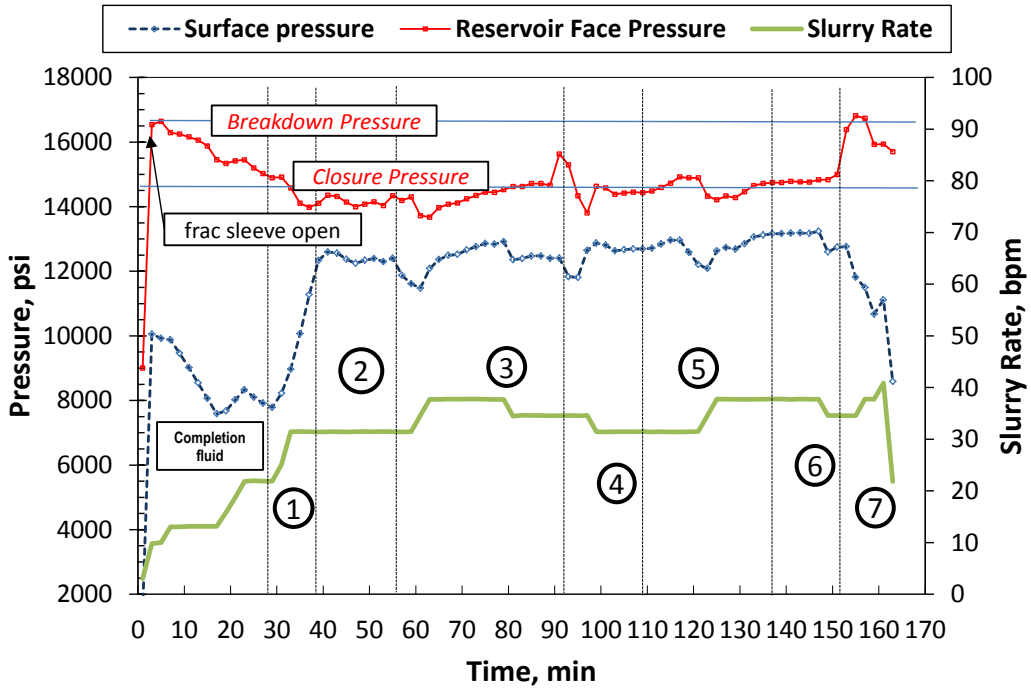

Fig. 44 Stage 1 treatment pressure & rate

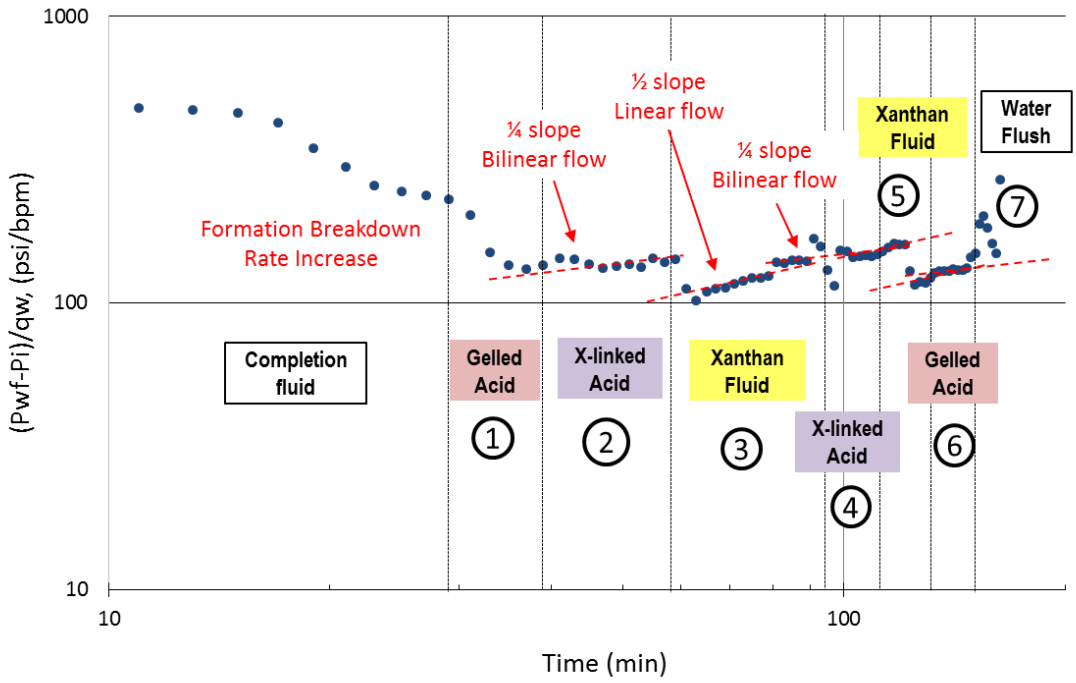

Fig. 45 Diagnostic plot to identify flow regimes.

Using treatment data in **Fig. 44**, the skin evolution when matrix acidizing is supposed and cross-sectional area growth when acid fracturing is supposed were computed as shown in **Fig. 46**.

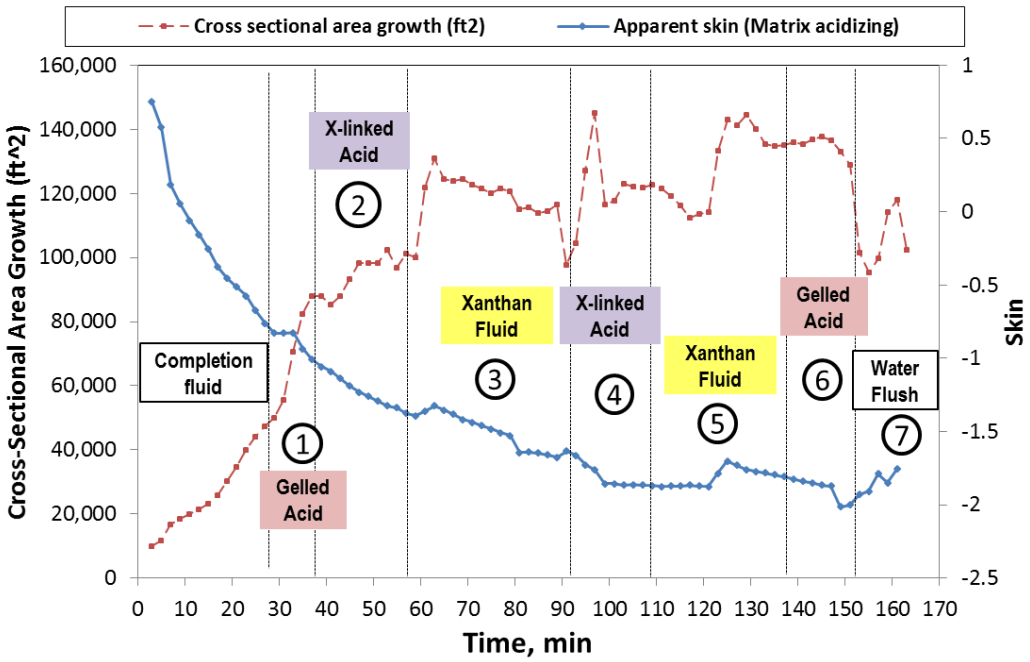

Fig. 46 Evolution of skin and cross-sectional area growth

From **Fig. 46**, it is observed that consistent cross-sectional area growth during the treatment. Strictly speaking from the diagnostic plot in **Fig. 45**, the area growth during xanthan frac fluid injection is not valid because the flow regime indicated fracture linear flow, ½ slope and further fracture extension. However, after fracture linear flow, it is noted that bilinear flow, ¼ slope followed the fracture linear flow and the cross-sectional area growth was monitored. Final cross-sectional area growth and skin before water flush are

100,000 ft^2 and -1.8 respectively. The equivalent fracture half-length is 140 ft, if fracture is assumed to be rectangular shape and the fracture height is 250 ft. uniformly.

3.3. Production Data Analysis after Acid Stimulation

When production data is available, it can be used to conduct a rate transient analysis (RTA). In our purposes, this analysis can be used to calculate cross-sectional area flowing from fractured wall, A_c and so that we can compare the calculated area between the stimulation and production so that the efficiency can be shown quantitatively in a field scale.

3.3.1. RTA Procedure for Gas Well

3.3.1.1. Generate the Specialized Plot

For dry gas reservoirs, the specific gravity of the gas sample obtained at the primary-separator conditions equals the value of a sample from the reservoir. However, for gas-condensate reservoir fluids, the specific gravities of gas samples taken from the reservoir and at the surface differ. By using recombination calculation, dry gas production was corrected to account for the condensate in the gas phase (Lee and Wattenbarger, 1996)

$$Q_{g,wet} = Q_{g,dry} + 133.316(\gamma_o Q_o / M_o) \tag{3.33}$$

From PVT report, oil in molecular weight is given. Thus, API and oil specific gravity is calculated.

$$API = \frac{5954}{M_o} + 8.811 \tag{3.34}$$

$$\gamma_o = \frac{141.5}{131.5 + API} \tag{3.35}$$

Recombined wet gas volume is used as production rate in this analysis. On the other hand, calculated bottomhole pressure in commercial RTA software is converted to real gas pseudo pressure and finally, $\Delta m(p)/q_g$ is obtained the square root of time plot is generated.

$$m(p) = 2\int_{p_o}^{p} \frac{p}{z\,\mu} dp \tag{3.36}$$

The production data, petrophysics, PVT, wellbore schematics, deviation survey etc. was loaded into commercial RTA software (fekete HARMONY) to obtain the bottomhole flowing pressure From the PVT report, reservoir is identified as gas condensate reservoir in this field case and recombined gas rate was calculated. Calculated bottomhole pressure was converted to pseudo pressure $m(p)$ and finally $\Delta m(p)/q_g$ vs. $\sqrt{t}$ plot was generated. For rate fluctuations due to operating changes, superposition time should be used.

$$\frac{m(p_i) - m(p_{wf})}{q_g} = \tilde{m}_4 \sqrt{t} + b \tag{3.37}$$

3.3.1.2. Diagnose the Specialized Plot

Read straight line slope from $\Delta m(p)/q_g$ vs. $\sqrt{t}$ plot and identify the time to the end of linear flow. Finally using Eq. (3.38) and (3.39), stimulated rock area and fracture half-length (x_f) is estimated from this plot and compared with real-time monitoring results.

$$\sqrt{k_m} A_{cm} = \frac{803.2T}{\sqrt{(\phi\mu c_t)_{f+m}}} \frac{1}{\tilde{m}_4} \tag{3.38}$$

Assuming stimulated rock volume to be uniform, x_f is calculated as follows:

$$x_f = \frac{A_{cm}}{4hn_f} \tag{3.39}$$

3.3.2. Case Study

3.3.2.1. Production History

The well in monitoring case study is used. The summary of production history is shown in **Fig. 47**.

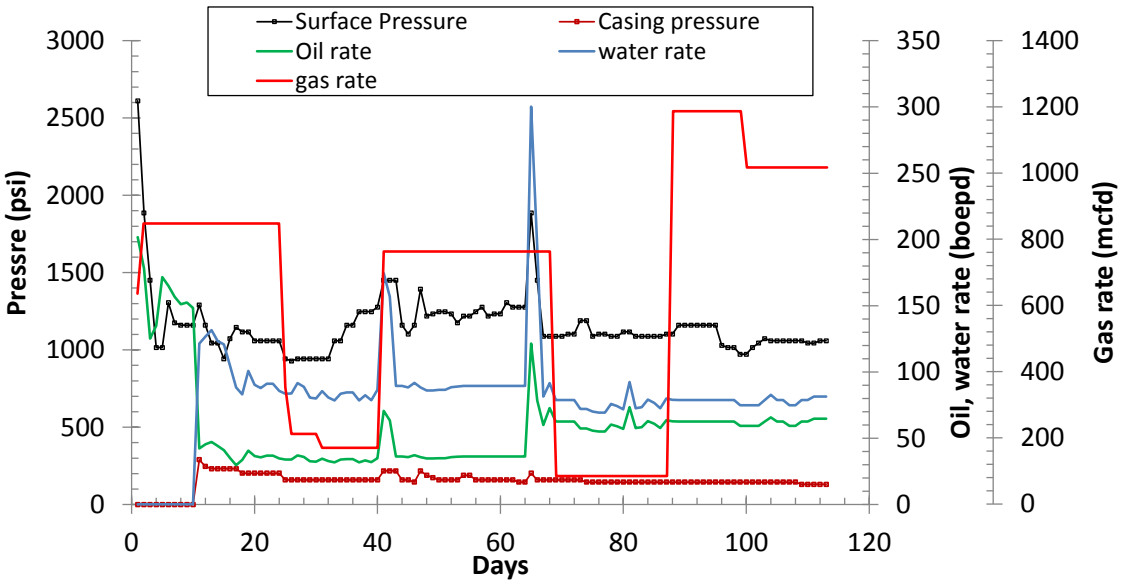

Fig. 47 Production history

As seen, in 113 days production, there was no shut-in during the period. Condensate, water as well as gas rate and surface pressure was recorded in surface. Choke size when well produced was 5 mm as constant during those periods. Along with methodology developed before, recombined gas rate and bottomhole pressure are calculated and shown in **Fig. 48**.

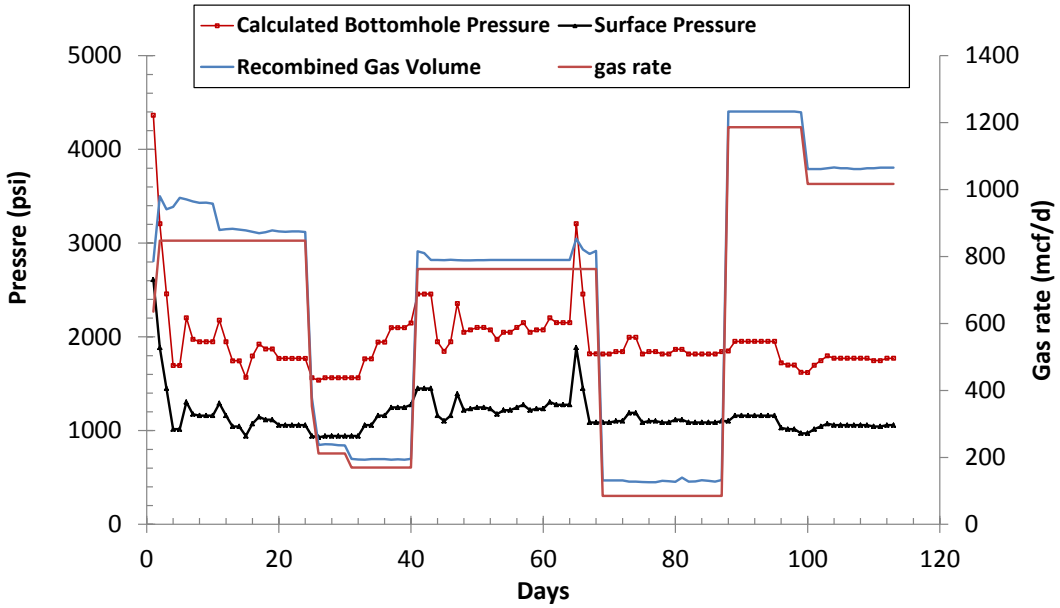

Fig. 48 Recombined gas rate and calculated bottomhole pressure

3.3.2.2. Production Analysis Result

Based on recombined gas rate and calculated bottomhole pressure, pressure normalized rate vs. material balance time in log-log scale is generated and plotted in **Fig. 49**.

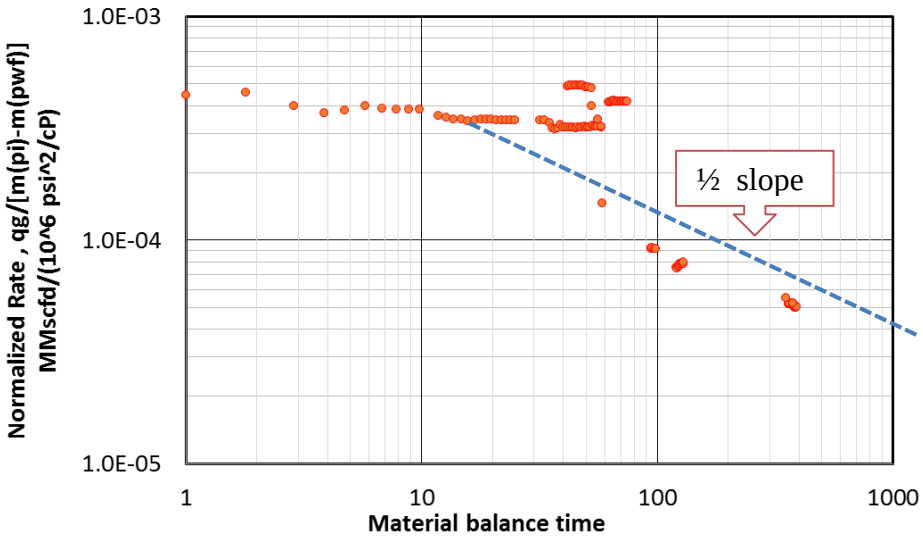

Fig. 49 Normalized rate vs. material balance time

Due to the low quality of data, it's not clear trend but half slope which indicates matrix linear flow is shown. Very early time indicates clean-up and the skin effects and it may mask early time behavior. As next step, square root time plot is generated in **Fig. 50**.

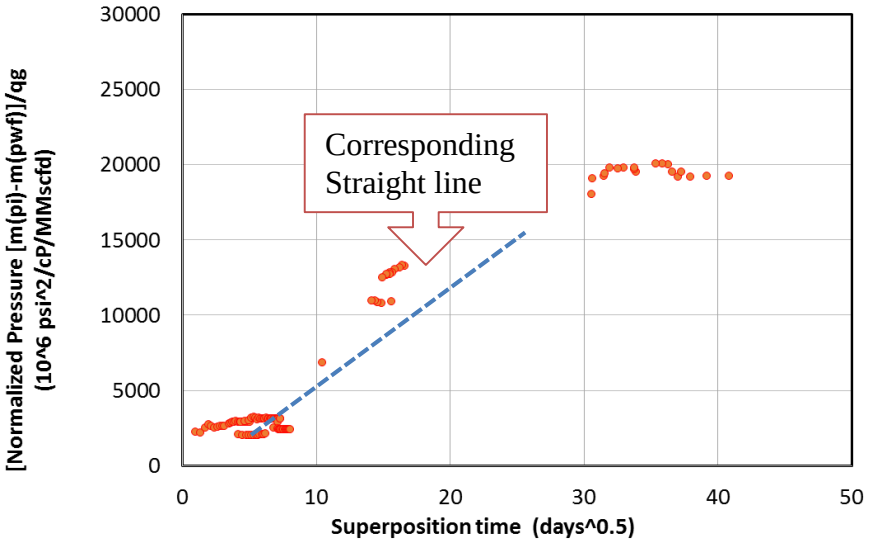

Fig. 50 Square root of time plot

The slop m_4 was read as $700000\ (700 \times 10^3)$. Now that the slope is known, $\sqrt{k_m}A_c$ should be calculated using Eq. (3.38). The constant values of **Table 13** are used for the calculation.

Table 13 Wellbore & stimulation data

Wellbore and stimulation assumptoin						
Course length	**# of frac**	**Effective spacing**	**Thickness**	**porosity**	**visicosity**	**ct**
ft		**ft**	**ft**		**cp**	**psi^-1**
3832	1	1357	250	0.03	0.0315	5.78E-05

Assuming the rectangular shape of fracture and 0.0044 md for matrix permeability that was obtained from the well log interpretation, cross-sectional area to flow in formation linear flow and uniform fracture half-length of each stage is calculated as below.

Table 14 Calculated fracture geometry

Summary of caluculation		
Ack^1/2	Acm	**xf**
md^0.5.ft^2	**ft^2**	**ft**
3581	53,990	54

Finally this area is compared with monitoring result shown in 3.2.5 and the summary is obtained in **Table 15**. It shows actual contributed area from flow is approximately half of stimulated area. This information may be helpful for optimization of next stimulation job.

Table 15 Comparison summary

Monitoring analysis	Production analysis	Efficiency
Stimulated area (ft2)	**Flowing area (ft2)**	**(Production/Stimulation)**
100,000	53,990	54%

4. CONCLUSION

In this thesis, integrated approach to evaluate both matrix acidizing and acid fracturing ("acid stimulation") has been implemented. Since, in many cases, once the acid reaches the formation, injection pressure cannot be kept above the formation closure stress, the fracture eventually closes, and the treatment becomes matrix acidizing rather than acid fracturing. Appropriate design and diagnostic method should be necessary to evaluate the treatment.

For matrix acidizing, using the existent numerical simulator and skin monitoring program, consolidating them into one package has been done. The package allows us to conduct acidizing design, monitoring the pressure and skin evolution and history match them and update uncertain parameters to use future treatment. Optimum rate schedule is also calculated based on the integrated approach.

For acid fracturing, the success of the treatment depends on many factors as to whether enough conductivity is secured, selected treatment works well in in-situ under specific geologic environment. Thus, observation and evaluation of past practice is critically important and inevitable step to develop further optimal stimulation procedures. We developed the methodology to conduct performance evaluation of acid fracturing treatment using treatment and production records.

The suggested integrated approach provides engineers with additional information as to whether the designed acid stimulation was performed appropriately under the in-situ

closure stress field. It is eventually helpful to look back past practice and enhance future stimulation.

REFERENCES

Agnia, A., Alkouh, A., and Wattenbarger, R. A. 2012. Bias in Rate-Transient Analysis Methods: Shale Gas Wells. Paper SPE 159710 presented at the SPE Annual Technical Conference and Exhibition, San Antonio, Texas, 8-10 October.

Al Ahmadi, H. A., Almarzooq, A. M., and Wattenbarger, R. A. 2010. Application of Linear Flow Analysis to Shale Gas Wells - Field Cases. Paper SPE 130370 presented at the SPE Unconventional Gas Conference, Pittsburgh, Pennsylvania, 23-25 February.

Bazin, B. 2001. From Matrix Acidizing to Acid Fracturing: A Laboratory Evaluation of Acid/Rock Interactions. SPE Production & Facilities 16 (1):22-29, SPE-66566-PA.

Bello, R.O. 2009. Rate Transient Analysis in Shale Gas Reservoirs with Transient Linear Behavior. PhD dissertation, Texas A&M University, College Station, Texas.

Bello, R. O. and Wattenbarger, R. A. 2010. Modelling and Analysis of Shale Gas Production With a Skin Effect. Journal of Canadian Petroleum Technology, 49(12), 37-48.

Ben-Naceur, K. and Economides, M. J. 1989. Design and evaluation of acid fracturing treatments. Paper SPE 18978presented at the SPE Low Permeability Reservoirs Symposium, Denver, Colorado, 6-8 March.

Buijse, M.A. and Glasbergen, G. 2005. A Semiempirical Model to Calculate Wormhole Growth in Carbonate Acidizing. Paper SPE 96892 presented at the SPE Annual Technical Conference and Exhibition, Dallas, 9-12 October.

Cohen, C.E., Ding, D., Quintard, M., Bazin, B. 2008. From porescale to wellbore scale: Impact of geometry on wormhole growth in carbonate acidization. Chem. Eng. Sci. 63 (12): 3088-3099.

Dong, K., Jin, X., Zhu, D., Hill, A.D. 2014. The Effect of Core Dimensions on the Optimal Acid Flux in Carbonate Acidizing. Paper SPE 168146 presented at the SPE International Symposium and Exhibition on Formation Damage Control, Lafayette, Louisiana, 26-28 February.

Economides, M.J., and Frick, T.P. 1994. Optimization of horizontal well matrix stimulation treatments. SPE Production & Facilities, 9(02), 93-99. SPE-22334-PA.

Economides, M.J., Hill, A.D., and Ehlig-Economides, C. 1994. PetroleumProduction Systems. Upper Saddle River, New Jersey: Prentice-Hall, Inc.

El-Banbi,A.H. 1998. Analysis of Tight Gas Wells. PhD Dissertation, Texas A&M University, College Station, Texas.

Elbel, J. L. 1994. Field Evaluation of Acid-Fracturing Treatments With Geometry Simulation, Buildup, and Production Data. SPE Production & Facilities, 9(01), 43-46, SPE-19773-PA.

Fredd, C.N. and Miller, M.J. 2000. Validation of Carbonate Matrix Stimulation Models. Paper SPE 58713 presented at the SPE International Symposium on Formation Damage Control, Lafayette, Louisiana, 23-24 February.

Furui, K., Burton, R.C., Burkhead, D.W., Abdelmalek, N.A., Hill, A.D., Zhu, D., and Nozaki, M. 2010. A Comprehensive Model of High-Rate Matrix Acid Stimulation for Long Horizontal Wells in Carbonate Reservoirs: Paper SPE 134265 presented at the SPE Annual Technical Conference and Exhibition, Florence, Italy, 19-22 September.

Goode, P. A. 1987. Pressure drawdown and buildup analysis of horizontal wells in anisotropic media. SPE Formation Evaluation, 2(04), 683-697. SPE-14250-PA.

Hill, A.D. and Zhu, D. 1996. Real-Time Monitoring of Matrix Acidizing Including the Effects of Diverting Agents. SPEPF11 (2): 95–101.

Izgec, O., Key, R., Zhu, D., and Hill, A.D. 2008. An Integrated Theoretical and Experimental Study on the Effects of Multiscale Heterogeneities in Matrix Acidizing of Carbonates. Paper SPE 115143 presented at the SPE Annual Technical Conference and Exhibition, Denver, 21-24 September.

Jackson, A.M., Azizi, B.A., Kofoed, C.W., Shuchart, C.E., Keller, S.R., Sau,R., Grubert, M.A., Phi, M.V. Completion and Stimulation Methodology for Long Horizontal Wells in Lower Permeability Carbonate Reservoirs. Paper SPE 161527 presented at Abu Dhabi International Petroleum Conference and Exhibition, Abu Dhabi, UAE, 11-14 November

Jawad, M.S. Al. 2014. Modeling of Acid Fracturing in Carbonate Reservoirs. Master of Science. Texas A&M University. College Station, Texas.

Kalfayan, L.J. 2007. Fracture Acidizing: History, Present State, and Future. Paper SPE 106371 presented at the SPE Hydraulic Fracturing Technology Conference, College Station, Texas, 29-31 January.

Kalia, N., and Balakotaiah, V. 2009. Effect of medium heterogeneities on reactive dissolution of carbonates. Chemical Engineering Science, 64(2), 376-390.

Kazemi, H. 1969. Pressure transient analysis of naturally fractured reservoirs with uniform fracture distribution. SPE J. 9(04): 451-462.. SPE-2156-A.

Kent, A.W., Burkhead, D.W., Burton, R.C., Furui,K., Actis,S.C., Bjornen,K., Constantine,J.J., Gilbert,W.W., Hodge,R.M., Ledlow, L.B., Nozaki, M., Vasshus, A., and Zhang, T. 2014. Intelligent Completion Inside Uncemented Liner For Selective High-Rate Carbonate Matrix Acidizing. SPE Drilling & Completion, 29(02), 165-181. SPE-166209-PA.

Lee, J., Wattenbarger, R.A. 1996. Gas Reservoir Engineering. SPE Textbook series Vol. 5.

McDuff, D., Jackson, S., Schuchart, C., and Postl, D. 2010. Understanding Wormholes in Carbonates: Unprecedented Experimental Scale and 3D Visualization. J Pet Technol 62 (10): 78-81. SPE-129329-MS.

Mishra, V., Zhu, D., Hill, A.D., and Furui, K. 2007. An Acid-Placement Model for Long Horizontal Wells in Carbonate Reservoirs. Paper SPE 107780 presented at the European Formation Damage Conference, Scheveningen, The Netherlands, 30 May-1 June.

Mostofizadeh, B. and Economides, M.J. 1994. Optimum Injection Rate From Radial Acidizing Experiments. Paper SPE 28547 presented at the SPE Annual Technical Conference and Exhibition, New Orleans, 25-28 September.

Paccaloni, G., Tambini, M., and Galoppini, M. 1988. Key Factors for Enhanced Results of Matrix Stimulation Treatments. Paper SPE 17154 presented at the SPE Formation Damage Control Symposium, Bakersfield, California.

Pandya, N.D. 2012. A Systematic Study of Matrix Acidizing Treatments Using Skin Monitoring Method. Master of Science. Texas A&M University. College Station, Texas.

Pournik, M., and Nasr-El-Din, H. A. 2010. Influence of Acid-Fracture Fluid Properties on Acid-Etched Surfaces and Resulting Fracture Conductivity. Paper SPE 128070 presented at the SPE International Symposium and Exhibition on Formation Damage Control, Lafayette, Louisiana, 10-12 February.

Prouvost, L.P. and Economides, M.J. 1989. Applications of Real-Time Matrix-Acidizing Evaluation Method. SPE Production Engineering 4 (4): 401-407. SPE-17156-PA.

Samandarli, O., McDonald, B., Barzola, G., Murray, M., and Richmond, P. 2014. Understanding Shale Performance: Performance Analysis Workflow With Analytical Models in Eagle Ford Shale Play. Paper SPE 169004 presented at the SPE Unconventional Resources Conference, The Woodlands, Texas, 1-3 April.

Sasongko, H., Zhu, D., and Hill, A. D. 2011. Simulation of Acid Jetting Treatments in Long Horizontal Wells. Paper SPE 144200 at the SPE European Formation Damage Conference, Noordwijk, The Netherlands, 7-10 June.

Tran, H.T. 2013. Modeling and Optimization of Matrix Acidizing in Horizontal Wells in Carbonate Reservoirs. Master of Science. Texas A&M University. College Station, Texas

Warren, J.E. and Root, P.J. 1963. The Behavior of Naturally Fractured Reservoirs. SPE J. 3 (3): 245-255. SPE-426-PA.

Zhu, D. and Hill, A.D. 1998. Field Results Demonstrate Enhanced Matrix Acidizing through Real-Time Monitoring. SPE Production & Operations 13 (4): 279-284. SPE-52400-PA

Zhu, D., Hill, A. D., and Looney, M. D. 1999. Evaluation of acid treatments in horizontal wells. Paper SPE 56782 presented at the SPE Annual Technical Conference and Exhibition, Houston, Texas, 3-6 October.

Zhu, D., Hill, A. D., and da Motta, E. P. 1998. On-site evaluation of acidizing treatment of a gas reservoir. Paper SPE 39421 presented at the SPE Formation Damage Control Conference, Lafayette, Louisiana, 18-19 February.